

WEIGHTED ENSEMBLE ANALYSIS OF EXTREME  
PRECIPITATION UNDER CLIMATE CHANGE

BY

CHEN ZHANG

THESIS

Submitted in partial fulfillment of the requirements  
for the degree of Master of Science in Civil Engineering  
in the Graduate College of the  
University of Illinois at Urbana-Champaign, 2016

Urbana, Illinois

Adviser:

Professor Ximing Cai

## Abstract

The frequency or intensity of heavy precipitation has likely increased in North America since 1950s. In order to analyze climate change impacts on extreme precipitation events in Chicago area, historical (1961-2000) and projected (2046-2065, 2081-2100) daily precipitation data are calculated from 13 statistical downscaling general circulation models under 3 CMIP3 emission scenarios: A1B, A2 and B1, as well as from 17 stations in NCDC and CCPN rain gage network. Then precipitation events of different recurrence intervals are calculated through regional frequency analysis and based on average deviation of climate model estimates from observation estimates, tricube weight function is used to assign weights to climate model ensemble. This weight result is further applied to projected quantile estimates to derive weighted expected values and confidence intervals of future extreme precipitation events under different emission scenarios, these results are further compared with current available estimates from NOAA Atlas 14. Finally, maximum entropy method (MEM) is applied to assign weights and the results are compared with those from weighted ensemble method (WEM). It is found that intensity and the confidence intervals of heavy precipitation is likely to increase significantly for about 20% from now to 2050s under all emission scenarios (A1B>A2>B1), afterwards, this increase trend will slow down (B1>A1B>A2). As for the performance of expected value projection based on MEM, it can also provide accurate estimates with high computational efficiency.

## Acknowledgements

The accomplishment of this work is attributed to the support from many people. I want to express my gratitude to my adviser Professor Ximing Cai and Dr. Momcilo Markus, who have provided insights, guidance and support for this research, from the initial ideas to the finalization of this thesis. I am also grateful to Greg Byard at Illinois State Water Survey and all members in Professor Cai's research group, for many great discussions and useful suggestions. Finally, special thanks to my parents, my girlfriend and "happy zoo family" for their mental support and encouragement during my graduate study.

## Table of Contents

Chapter 1 Introduction .....	1
Chapter 2 Methodology: Regional Frequency Analysis of Chicago Region .....	12
Chapter 3 Weighted Ensemble Analysis and Uncertainty Assessment .....	24
Chapter 4 Weighted Ensemble Analysis Based on Maximum Entropy Method .....	34
Chapter 5 Conclusions.....	39
Chapter 6 Figures .....	44
Chapter 7 Tables.....	68
References .....	86

# Chapter 1 Introduction

## 1.1 Background

Climate change, perhaps one of the most popular “key word” in both academia and social media, has become an important issue over the past decades, both socially and scientifically. Intensive human activities have increased atmospheric concentrations of greenhouse gases such as carbon dioxide (CO<sub>2</sub>), methane (CH<sub>4</sub>), nitrous oxide (N<sub>2</sub>O) and then interfered global energy and water circulation system. Environmental impacts such as temperature anomaly, water scarcity, intense extreme events have brought many threats to the whole world through the combination of societal impacts such as population increase, food availability etc. [Kotir, 2011]. In the past century, anthropogenic greenhouse gas emissions has increased rapidly and observed global temperature has increased 0.76 Celsius degree from 1906 to 2005. If we look at the recent 50-year within this period, the increasing speed even doubled [Change, 2007]. Besides, due to the melting of glaciers, the global sea surface level has risen at a rate of 1.8mm per year from 1961 to 2003 and this speed went up to 3.1mm per year during 1993 to 2003 [Change, 2007]. In particular, climate change is likely to bring more extreme precipitation events [Allan and Soden, 2008]. IPCC states that extreme events such as floods and droughts are likely to be more frequent and intense [Change, 2007], it will further modify the evaporation and soil water storage patterns and finally alter the whole hydrological system [Olesen and Bindi, 2002]. Besides the temporal variability of climate change effects, they also vary significantly under

spatial scale. IPCC reports that from 1900 to 2005, northern and central Asia, northern Europe and eastern shore of North and South America have experienced most significant precipitation increases while in Sahel, southern Africa and Mediterranean, significant declines have been observed [*Change*, 2007].

One might ask such a question: How do people track the change of meteorological data during the past, and predict those for the future, with limited or even unknown data? The answer usually lies in a simulation model, namely general circulation model (GCM). Generally speaking, a GCM aims to describe atmospheric and oceanic climate behaviors through the integration of physical or empirical equations with a global coverage but a coarse spatial resolution. As human GHG emissions are also parts of model inputs, GCMs can be run under different emission scenarios to simulate and predict human activity impacts on climate variables such as precipitations and temperatures. In some international climate change assessment reports, the Intergovernmental Panel on Climate Change (IPCC) collected and analyzed a group of GCMs. The model ensemble is called Climate Model Intercomparison Project (CMIP), which has served as an important tool for climate change assessment [*Meehl et al.*, 2007]. CMIP3 was used for IPCC's fourth assessment report (AR4) published in 2007, while CMIP5 was used for the fifth assessment report (AR5) published in 2013. CMIP5 and CMIP3 both generate projections of future climate scenarios. However in terms of the description of human GHG emission scenarios in the future under different social development conditions, they have different standards. CMIP3 uses emission scenarios that were described in IPCC's Special report on Emission

Scenarios (SRES). There are four families in total: A1, A2, B1, B2. Additionally, There are four scenarios groups within A1: A1C, A1G, A1B and A1T. Four families have different storylines. A1 describes a future world with rapid economic growth, rapid introduction of new and efficient technologies but low population growth. A2 describes a very heterogeneous world where population growth is high but technology changes are slower compared to other storylines. B1 describes a convergent world with low population growth and rapid changes in economic structures toward resource-efficient way. B2 describes a world with moderate population growth, intermediate economic development level and diverse technological change. The corresponding CO<sub>2</sub> emissions of CMIP3 is shown in Figure 1. CMIP5 takes radiative forcing scenarios named representative concentration pathways (RCPs). It takes into account the impact of atmospheric concentrations of GHG as well as aerosols and the unit is watts per square meter. There are four levels of RCPs in total: one low forcing level (RCP2.6), two medium level (RCP4.5 and RCP6) and one high emission level (RCP8.5) [Nakicenovic and Swart, 2000]. The corresponding CO<sub>2</sub> concentration of CMIP5 and the comparison with CMIP3 is shown in Figure 2 and 3. We should notice that compared to SRES scenarios, RCP levels have a wider range of possible future emission scenarios and RCP8.5, the highest one, is comparable to the highest SRES scenario. As for the performance of CMIP3 and CMIP5, though CMIP5 incorporates newer emission scenarios, and more sophisticated GCMs, thus CMIP5 is becoming the de facto standard for projections [Ray et al., 2008]. However it does not necessarily guarantee that CMIP5 outperforms CMIP3 in every aspect. [Flato et al., 2013] says: “There is medium evidence

(single multi-model study) and medium agreement (as inter-model difference is large) that CMIP5 models tend to simulate more intense and thus more realistic precipitation extremes than CMIP3, which could be partly due to generally higher horizontal resolution. There is medium evidence and high agreement that CMIP3 models tend to underestimate the sensitivity of extreme precipitation intensity to temperature.” [Kunkel et al., 2015] suggest both CMIP3 and CMIP5 should be used since CMIP3 has already been validated and endorsed. In our study, we pre-processed annual maximum series of precipitation data from two data sources: one under CMIP3 and another under CMIP5, CMIP3 dataset is less biased therefore it was selected.

As mentioned earlier, the spatial resolution of GCMs is too coarse to solve sub-grid scale problems [Grotch and MacCracken, 1991]. Salathe gives us an example, the grid size of GCM model named HadCM3 is 2.5 latitude by 3.75 longitude. However, in order to run monthly flow simulation in mountainous catchments, at least a resolution of 0.125 degree is required [Salathé, 2003]. In order to get more accurate information on a regional scale, downscaling methods have been used to explore the impact assessment of climate change on hydrological processes [Robert L. Wilby et al., 2002; Xu, 1999]. Detailed reviews of downscaling methods can be found from [Hanssen-Bauer et al., 2005; Hewitson and Crane, 1996; Robert L. Wilby and Wigley, 1997; R. L. Wilby et al., 2004; Zorita and Von Storch, 1999]. It consists of two fundamental categories: dynamical downscaling and statistical downscaling. Dynamical downscaling is based on the modeling of physical process, and usually a regional climate model (RCM) with higher resolution is coupled with GCM. GCM could provide large-scale and lateral boundary conditions to RCMs in



finer resolution to simulate regional hydrological processes more realistically [Fowler *et al.*, 2007]. However, dynamical downscaling is quite computationally expensive and only a limited number of dynamical downscaling models are available. Statistical downscaling, on the other hand, simply relies on the statistical relationship between large-scale parameters from GCMs and local meteorological values, this relationship could be derived through observation data series [Nguyen, 2005; Xu, 1999]. It can be further classified into three subgroups: regression models, weather generators and weather typing schemes [Fowler *et al.*, 2007]. Compared to dynamical downscaling, statistical downscaling is computationally efficient and can provide us variables that are not included within RCM. There are also more available statistical downscaled GCMs, which is very useful in the formulation of weighted ensemble. Adapted from Wilby and Wigley [Robert L. Wilby and Wigley, 1997], Fowler provides a summary of advantages and disadvantages of statistical downscaling and dynamical downscaling in Table 1 [Fowler *et al.*, 2007].

Researchers have developed over 20 GCMs to simulate and predict climate change impact under global scale [Zhang, 2010]. However, the simulation results from some models vary a lot or even are in conflict to each other under a regional scale [Laurent and Cai, 2007]. There are two possible reasons. Firstly, forcing data varies between models [Flato *et al.*, 2013]. Secondly, climate sensitivities are different for different GCMs [Sanderson *et al.*, 2015]. Thus instead of “putting eggs in one single GCM”, model ensemble can provide us reliable estimate of climate change impact in the future [Murphy *et al.*, 2004]. Researchers pointed out that CMIP3 models

are not mutually independent [Jun *et al.*, 2008; Pennell and Reichler, 2011], this situation also exists in CMIP5 model ensemble, Benjamin argued that this collection of models share duplicated codes, same forcing and validation data which may bring bias in estimation and spurious correlations. Therefore, simply averaging all models neglects the variation of model quality [Murphy *et al.*, 2004], weighted model results are able to form more accurate and reliable climate change projections [Gleckler *et al.*, 2008]. Some model metrics can be relied on to make quantitative judgments on how to use information from a collection of models for a particular application [Annamalai *et al.*, 2007]. Many researchers applied this weighted ensemble idea in hydrological and meteorological studies. [Wehner, 2013] analyzed ensemble of NARCAPP climate models and projected mid-century changes in seasonal precipitation extremes. [Nohara *et al.*, 2006] investigated river discharge projection for 24 major rivers in the world through 19 coupled AOGCMs under A1B scenario. [Gain *et al.*, 2011] applied discharge-weighted ensemble modeling and detected trends in high and low flows at lower Brahmaputra for the next century. [Tramblay *et al.*, 2012] used 15 RCMs to analyze climate change impacts on extreme precipitation in Morocco. However, few studies have touched comprehensive uncertainty analysis of weighted ensemble results, the uncertainty arises from many aspects, such as different projected emission scenarios, different model projections, parameter or sampling uncertainty within single model realization.

In urban areas, the parameters of the design storm precipitation are calculated by statistical analysis of rain gage data, and then spatially interpolated to create isohyetal maps [Bonnin *et al.*,

2006]. Afterwards, storm sewers, sizing of bridges, and determination of flood inundation areas are designed or updated using extreme event design storms provided above [Winters *et al.*, 2015]. Researchers have been focusing on the projection of extreme events for a long time. As the concentration of GHG increases, the increase of precipitation intensity in future climate scenario was one of the major findings from early models, and this finding remains proved by more sophisticated models afterwards [Hennesy *et al.*, 1997; Kothavala, 1997]. This change has been recognized to have geographical dependence [Meehl *et al.*, 2000]. For example, In south Asian monsoon region, the range of precipitation intensity increases under future climate scenario, the west part will experience a decrease of extreme precipitation while the east part will experience an increase [Bhaskaran and Mitchell, 1998]. In the United States, nested regional model has projected an increase in extreme precipitation events [Giorgi *et al.*, 1998]. Under regional perspective, [Kim, 2005] used dynamically downscaled dataset to analyze extreme hydrologic events in the western United States and found that they are very likely to increase in 2050s and the largest increases would happen in the mountainous regions of the northern California. [Rajczak *et al.*, 2013] used RCM ensemble to project extreme precipitation events in Europe and the Alpine region, they found an increase in Northern Europe but an decrease in Southern Europe in 2100s. Recently, [Schuster *et al.*, 2011] used statistically-downscaled and de-biased precipitation projections for the state of Wisconsin derived from 14 General Circulation Models (GCMs) to assess the projected precipitation changes for the mid-21st century. They found that the potential impacts of climate change on

extreme hydrologic events were projected to increase in the Midwest, particularly in the vicinity of Chicago. However, statistical analyses under current standards, such as those published in Atlas 14 [Bonnin *et al.*, 2006], are based on the following assumption: precipitation time series is stationary and climate change impact is not considered. On the other hand, some researchers (e.g., [Markus *et al.*, 2007]) have already detected trends in heavy rainfall observations and adjust for it [Huff and Angel, 1989]. Therefore, using only statistics of the past observed rainfall will likely underestimate future storms and floods as well as confidence intervals, which will pose urban drainage infrastructure design under risk. Our goal in this study is to take advantage of downscaled climate model ensemble to investigate climate change impacts on future extreme precipitations, provide robust weighted quantile estimates, and propose methods for uncertainty analysis and confidence interval estimates. Cook County, a highly urbanized area, was selected as our area of interest to illustrate the whole framework.

## **1.2 Dataset Description**

Observed rainfall data in this research were reviewed and acquired from the National Oceanic and Atmospheric Administration (NOAA) National Climate Data Center (NCDC) [NOAA] and the Cook County Precipitation Network (CCPN) from Illinois State Water Survey (ISWS) [ISWS]. Sites of interests were selected based on spatial coverage, period of record, data quality and completeness. In order to be consistent with the temporal coverage of climate model data introduced later, daily rainfall observation during 1961-2000 from 12 stations were processed from NCDC dataset to obtain annual maximum series (AMS). In order to provide comprehensive

spatial coverage of our interest area, 5 more stations from CCPN were added to provide AMS of daily rainfall from 1989 to 2000 due to data availability. A whole list of station names and properties as well as station distribution map are described in Figure 4 and Table 2.

Two sources of climate data were selected in this research and the model names are listed in Table 3 and Table 4:

a) CMIP5-Dynamically Downscaled-Oak Ridge National Lab (ORNL), described in [Oubeidillah *et al.*, 2014] and [Ashfaq *et al.*, 2010; Ashfaq *et al.*, 2013]. This dataset includes 10 dynamically downscaled GCM results of daily precipitation, both in historical period and future period under one CMIP5 climate scenarios (RCP8.5), spatial resolution is 0.0417 degree.

b) CMIP3-Statistically Downscaled-University of Wisconsin-Madison (UW) [Notaro *et al.*, 2014]. This dataset includes 13 statistically downscaled GCM results (3 realizations per each GCM) of daily precipitation, both in historical period (1961-2000) and two future periods (2046-2065 and 2081-2100) under three different CMIP3 climate scenarios (A1B, A2 and B1), spatial resolution is 0.1 degree.

Grid precipitation data corresponding to station (point) precipitation data were extracted from original dataset and processed to get AMS of daily rainfall for further analysis. It should be noted that CMIP3-Statistically Downscaled dataset is more favored for the following reasons:

a) More GCM model runs, which is favorable during weighting procedure described in methodology section.

b) More climate scenarios and longer temporal coverage, which is favorable in analyzing

climate change effects during mid-21 century and late-21 century.

- c) After initial comparison of model AMS with observation AMS, this dataset is less biased compared to ORNL dataset, taking O'hare Airport station as an example, AMS of daily precipitation at ORNL are plotted in Figure 5.

Therefore in our final results, weighted precipitation estimates, confidence intervals and isoheytal maps are all based on CMIP3-Statistically Downscaled dataset.

### **1.3 Thesis objective and outline**

The overall objective of this research is to understand how different climate change scenarios will affect the precipitation events with different recurrence intervals in the Great Chicago Region during 2050s and 2100s. It could serve as a reference for municipal facility design, civil infrastructure reliability analysis and further analysis of flow generation procedure in urban areas etc. Using statistically downscaled GCM climate data and observation data in historical period (1961-2000), a weighted model ensemble approach will be applied instead of simply average different model results. Thus model performance in estimating extreme precipitation events could be assessed. Isoheytal maps for design precipitation will be provided as one type of final results. Besides, this research will more emphasize the confidence intervals of the precipitation event estimates. In NOAA Atlas 14, confidence intervals were also reported, but only being able to reflect parameter uncertainty in a curve-fitting procedure. In this research, we will propose a new method to calculate confidence intervals that could take into account both parameter uncertainty (sampling uncertainty) and model uncertainty. Isoheytal maps for

confidence intervals will also be provided. Finally, in addition to using traditional weighting functions to determine model ensemble weights, maximum entropy method (MEM) will be introduced and used to provide another set of precipitation event estimates. The two sets of results are compared.

The chapters of thesis are organized as follows:

Chapter 2 describes the methodology of extreme precipitation event estimation with regional frequency analysis, assessment of climate model performance and weight determination of weight ensemble model framework, and construction of confidence intervals from Monte Carlo simulation.

Chapter 3 mainly discusses weight calculation results, precipitation event estimates under different climate scenario in two different future periods, definition of different confidence intervals and the result comparison among the the outputs from this study and those estimates available from NOAA Atlas 14.

Chapter 4 provides an overview of maximum entropy method (MEM) and an application in this study; results of precipitation event estimates are then compared with those from the weighted ensemble approach.

Chapter 5 discusses the conclusions and limitations of this research, as well as the future scope of study.

## Chapter 2 Methodology: Regional Frequency Analysis of Chicago Region

Estimating the frequency of extreme events with different recurrence intervals at different sites is of great importance. However, data coverage at one particular site might not be long enough to provide a robust estimate of recurrence intervals, especially for extreme events. If within a region, event frequencies follow the same distribution among different sites, then temporal insufficiency in datasets can be complemented by spatial coverage, and more accurate estimates can be reached by analyzing the whole data samples as a group other than only data from single site [Jonathan Richard Morley Hosking and Wallis, 2005]. This approach takes the idea of “temporal and spatial conversion” and is known as “regional frequency analysis”.

In this chapter, a detailed description of region frequency analysis is introduced, particularly on the formation of region of the study area based on downscaled model results (AMS for different sites), discordancy and heterogeneity measurement of sites, determination of best-fit curve and event estimates based on L-moments. More definitions and deviations can be found in the book *Regional frequency analysis: an approach based on L-moments* [Jonathan Richard Morley Hosking and Wallis, 2005]. Then, the method to obtain corresponding weights for the model ensemble is described, therefore weighted ensemble mean value can be derived as the best estimate of extreme events. Finally, a novel method to assess the uncertainty of extreme events is introduced, which could combine the uncertainty from the curve fitting procedure and uncertainty from the model ensemble and thus provide a robust and comprehensive assessment of confidence intervals for extreme events in the future under different climate



change scenarios.

## 2.1 Regional Frequency Analysis (RFA) Based on L-moments

Two key words should be emphasized in RFA, namely “regional” and “frequency”. “Regional” indicates the definition of a single homogeneous region and the index flood procedure is applied using data from  $N$  sites and each site  $i$  composed of the sample size of  $n_i$  ( $n_i$  years of data in this study). Denoting  $Q_{ij}$  as the annual maximum daily precipitation at site  $i$  in year  $j$ , supposing  $Q_i(F)$  is the quantile function of frequency distribution at site  $i$  ( $0 < F < 1$ ), we can write:

$$Q_i(F) = m_i * q(F) \quad (2.1)$$

The underlying assumption is that, those sites could form a homogeneous region where the frequency distributions of  $N$  sites are identical apart from a scaling factor  $m_i$  that is site specific, the index flood [Jonathan Richard Morley Hosking and Wallis, 2005]. In this study,  $m_i$  is estimated as the mean value of AMS at site  $i$ . The second word, “frequency”, indicates curve fitting to known data points.  $q(F)$  is the quantile function of regional frequency distribution, also denoted as regional growth curve. The form of  $q(F)$  can be assumed to have  $p$  unknown parameters, which can be estimated from higher order moment statistics from a regional perspective. Naturally, we can speculate that the “regional moment” is a weighted form of site statistics, and details will be introduced in later parts.

The most important mathematic tool used in this study is L-moments. Traditionally, the shape of probability distribution can be determined by moments of distribution including mean, variance, skewness etc. The mean is defined as

$$\mu = E(X) \quad (2.2)$$

Higher order moments are defined as

$$\mu_r = E(X - \mu)^r, r = 2, 3, \dots \quad (2.3)$$

Following are additional useful definitions

$$\text{standard deviation } \sigma = \mu_2^{\frac{1}{2}} \quad (2.4)$$

$$\text{coefficient of variation (CV)} = \frac{\sigma}{\mu} \quad (2.5)$$

$$\text{skewness } \gamma = \mu_3 / \mu_2^{3/2} \quad (2.6)$$

$$\text{kurtosis } \kappa = \mu_4 / \mu_2^2 \quad (2.7)$$

However, [J. R. M. Hosking and Wallis, 1993] found that for skew distributions, parameter inferences based on traditional sample moments are likely to be biased and thus unreliable. A more desirable measurement of distribution shape can be obtained from another set of language: L-moments.

L-moments are modifications of “probability weighted moments” [Greenwood et al., 1979]. For a random variable X with a cumulative distribution function F(.), the probability weighted moments are defined as

$$M_{p,r,s} = E[X^p \{F(X)\}^r \{1 - F(X)\}^s] \quad (2.8)$$

Special cases such as  $\alpha_r = M_{1,0,r}$  and  $\beta_r = M_{1,r,0}$  are very useful in the definition of L-moments.

For a random variable X with quantile function x(p), L-moments of X are defined as

$$\lambda_r = \int_0^1 x(p) P_{r-1}^*(p) dp \quad (2.9)$$

where

$$P_r^*(p) = \sum_{k=0}^r p_{r,k}^* p^k \quad (2.10)$$

and

$$p_{r,k}^* = (-1)^{r-k} \binom{r}{k} \binom{r+k}{k} \quad (2.11)$$

Following the definition above, the first to fourth order of L-moments are given below

$$\lambda_1 = \alpha_0 = \beta_0 \quad (2.12)$$

$$\lambda_2 = \alpha_0 - 2\alpha_1 = 2\beta_1 - \beta_0 \quad (2.13)$$

$$\lambda_3 = \alpha_0 - 6\alpha_1 + 6\alpha_2 = 6\beta_2 - 6\beta_1 + \beta_0 \quad (2.14)$$

$$\lambda_4 = \alpha_0 - 12\alpha_1 + 30\alpha_2 - 20\alpha_3 = 20\beta_3 - 30\beta_2 + 12\beta_1 - \beta_0 \quad (2.15)$$

*( $\lambda_1$  is L – location,  $\lambda_2$  is L – scale)*

Similar to the coefficient of variance, coefficient of skewness etc., L-moment ratios can be used

as tools to describe the shape of distribution as follows:

$$\tau_r = \frac{\lambda_r}{\lambda_2}, r = 2, 3, 4 \dots \quad (2.16)$$

*( $\tau_3$  is L – skewness and  $\tau_4$  is L – kurtosis)*

Particularly, L-CV is defined as

$$\tau = \lambda_2 / \lambda_1 \quad (2.17)$$

Two properties of L-moments are very important. The first is existence: If distribution mean exists, all of L-moments exist. The second is uniqueness: If distribution mean exists, no two distributions have the same L-moments. Comparing to traditional moments, higher orders of L-moments are still linear combinations, which could suggest L-moments results are more

robust to observation errors since they will not propagate quadratically or cubically [J. R. M. Hosking and Wallis, 1993]. Parameters in different distributions have explicit expressions from L-moments ratios, thus through calculation of sample L-moments, we can fit different distribution curves to data points.

There are four steps in RFA, which are described as follows:

- Data screening

As we can expect, data screening is probably the first step for every type of analysis. Through inspection of AMS of precipitation at every site, errors and inconsistencies are removed or replaced. Despite the properties in data itself, external information should also be used including measurement method, site location change etc., to make sure that data are trustworthy for determination of regional frequency distribution. In this study, besides external information, a statistical method using properties in data itself was applied to finding and removing site outliers, namely discordancy measurement [Jonathan Richard Morley Hosking and Wallis, 2005]. Discordancy is measured through L-moments of sites' AMS. Procedures are described below.

Firstly, sample L-CV, L-skewness and L-kurtosis for every site were calculated. These results can be regarded as coordinates of a particular point in a three-dimensional space. Heuristically, if one point is "too far away from the center of the group", it is "discordant" and should be removed.

Secondly, as described by Hoskin and Wallis, supposing totally there are  $N$  sites, for site  $i$ , vector

$u_i = [t^i, t_3^i, t_4^i]^T$  contains L-CV, L-skewness and L-kurtosis information, discordancy measure  $D_i$  is then defined as follows:

$$U = N^{-1} \sum_{i=1}^N u_i \quad (2.18)$$

$$A = \sum_{i=1}^N (u_i - U)(u_i - U)^T \quad (2.19)$$

$$D_i = \frac{1}{3} N (u_i - U)^T A^{-1} (u_i - U) \quad (2.20)$$

If  $D_i$  is very large, site  $i$  is discordant. We should notice that the threshold of “large” is dependent on  $N$ , the number of sites. Detailed relationship can be found in Table 3.1 of Hoskins and Wallis (year). In our study, the total site number is greater than 15, and the critical value of  $D_i$  is 3.

- Identify homogeneous region

As we mentioned earlier, one important assumption in index flood method is that sites could form a homogeneous region, thus identification of homogenous region is very important. A large study region could be divided into several small homogeneous regions based on other physical properties such as altitude, vegetation, soil type etc. and then justified or modified by homogeneity criterion [Jonathan Richard Morley Hosking and Wallis, 2005]. However in this study, considering the small spatial coverage of our study region, we pre-assume the study region is homogeneous. Firstly we select a group of stations to form the region, and then homogeneity criterion is applied to testing whether our selection is valid. If not, we delete or add stations until homogeneity criterion is to some extent satisfied. Heterogeneity measure  $H$  will again take advantage of L-moments statistics and the formation of  $H$  will be described in the

following part.

Ideally, within a perfect homogeneous region, all sites would have the same L-moments ratios under the assumption that the site frequency distributions are identical apart from a scaling factor. However, it will never be true, our question is whether the dispersion of frequency distributions among different sites is acceptable to form a homogeneous region. Thus a measure of between-site dispersion was established based on site L-moment ratios.

Firstly, an artificial region was constructed. It has the same number of sites, length of records and site L-moments ratios. Then regional L-moments ratios were calculated, and based on these values, a Kappa distribution (4 parameters) was fitted to describe extreme events of this artificial region. Afterwards, a large number ( $N_{\text{simu}}$ ) of realizations were simulated based on the kappa distribution, noting that this simulation is conducted in the artificial region that is perfectly homogeneous. Finally we compare the deviations of L-moments ratios between the real case and the artificial case to find whether our true region can be accepted as homogeneous. The mathematical forms are described below:

$$\text{regional } L - \text{moment ratios: } t^R = \sum_{i=1}^N n_i t^i / \sum_{i=1}^N n_i \quad (2.21)$$

$$V = \left\{ \sum_{i=1}^N n_i (t^i - t^R)^2 / \sum_{i=1}^N n_i \right\}^{1/2} \quad (2.22)$$

$$H = \frac{V - \mu_V}{\sigma_V} \quad (2.23)$$

where  $\mu_V$  and  $\sigma_V$  are mean and standard deviation of  $N_{\text{simu}}$  values of  $V$ , respectively.

If  $H$  is very large, the region is determined to be heterogeneous. Hoskin and Wallis suggests the region be regarded as “acceptably homogeneous” for  $H < 1$  and “possibly heterogeneous” if

$1 < H < 2$ . In this study, we decided  $H=2$  as the threshold between “homogeneous” and “heterogeneous”.

- Choose the best-fit frequency distribution

When determining expected values of extreme precipitation events, one single frequency distribution is fitted to data within a single region. Since in reality, the whole region will never be perfectly homogeneous, our aim is to find such a distribution that could give accurate quantile estimates for all sites. Similar to the identification of homogeneous region, region L-moments ratios are first calculated. Then, a set of three-parameter distributions are selected as our candidates, including generalized logistic (GLO), generalized extreme value (GEV), generalized pareto (GPA), lognormal (GNO) and Pearson type III (PE3). With the information of regional L-moments 1 (regional mean),  $t^R$  and  $t_3^R$ , we can fit each candidate distribution and calculate the L-kurtosis of the fitted distribution, denoted as  $t_4^{dist}$ . Furthermore, with the information of regional L-moments 1 (regional mean),  $t^R$ ,  $t_3^R$  and  $t_4^R$ , we fit a kappa distribution and then simulate  $N_{simu}$  of realizations. Each realization represents a perfect homogeneous region where neither serial correlation nor site-cross correlation exists, regional average L-skewness and L-kurtosis are also calculated in each realization, denoted as  $t_3^m$  and  $t_4^m$ , respectively. For each distribution, the goodness to fit measure is defined as follows

$$Z^{dist} = (t_4^{dist} - t_4^R + B_4) / \sigma_4 \quad (2.24)$$

where

$$B_4 = N_{simu}^{-1} \sum_{m=1}^{N_{simu}} (t_4^m - t_4^R) \quad (2.25)$$

and  $\sigma_4$  is the standard deviation of  $t_4^R$ .

The closer  $Z^{dist}$  approaches to zero, the better the frequency distribution fits. As Hoskin and Wallis mentioned, a reasonable threshold would be  $|Z^{dist}| \leq 1.64$ . In this study, only the best one from the five candidate distributions was used to calculate the expected values of precipitation quantiles.

- Estimate the frequency distribution

Recall the basic equation mentioned at the very beginning of this section

$$Q_i(F) = m_i * q(F) \quad (2.26)$$

$q(F)$  is the quantile function of regional frequency distribution and has already been determined from best-fit distribution curve.  $m_i$ , the index flood, is estimated as the mean value of AMS at site  $i$ . Therefore, we can easily derive different precipitation quantiles at different sites within our study region, both for quantiles from observation values and from climate models. These quantiles are then assessed in the following weight determination procedure and can be used as input to derive weighted ensemble quantiles. The aforementioned procedures were proceeded by R language, with R package *lmomRFA* [J. R. M. Hosking, 2015].

## 2.2 Weight Determination for Model Ensemble

Precipitation frequency estimates of an 24-hour event were derived for a range of frequencies using RFA based on L-moment statistics as described in previous section, noting that these estimates were calculated from annual maximum series (AMS).

The return period is also referred to as the average recurrence interval (ARI). The “true” average



recurrence interval (ARI) between exceedance of a particular magnitude of event is calculated through frequency analysis based on partial duration series (PDS). Differences in analysis results based on AMS and PDS are negligible if ARI greater than 15-year (Atlas 14, Volume 9). But for smaller ARIs, Langbein's formula [Langbein, 1949] was used to transform PDS-based average recurrence interval (ARI) to AMS-based annual exceedance probability (AEP):  $AEP=1-\exp(-1/ARI)$ . Thus after conversion, equivalent frequencies used in this study are: 2.54-year, 5.52-year, 10.51-year, 25-year, 50-year, 100-year corresponds to 2-year, 5-year, 10-year, 25-year, 50-year, 100-year.

Precipitation frequency estimates from downscaled models were compared with estimates from observations for ensemble analysis. Since model estimates were based on grid data while observation estimates were based on point data, an empirical conversion factor was introduced to get comparable results [Lynch, 1998]. This factor is related to grid size and event duration. In our study, point-to-grid conversion factor was chosen as 0.96.

In the next step, model estimates were compared with estimates from observation data to determine model weights in ensemble analysis. Weights were determined using a tricube weight function (Mosteller and Tukey, 1977):

$$w = \begin{cases} \left(1 - \left(\frac{|d|}{h}\right)^3\right)^3, & \text{if } |d| \leq h \\ 0, & \text{if } |d| \geq h \end{cases} \quad (2.27)$$

$w$  is the weight for a particular model, and  $d$  is the average percent deviation of a particular model from observation estimates:

$$d = \frac{\sum_{i=1}^{n_{station}} \sum_{j=1}^{n_{event}} \frac{model_{i,j} - obs_{i,j}}{obs_{i,j}} * 100\%}{n_{station} * n_{event}} \quad (2.28)$$

where h is the half window width defined as one standard deviation of the whole series of average percent deviation for different models. Weights for different model estimates were normalized to the scale of 1 to determine the weighted frequency estimates. It is noticed that the majority of AMS daily data was taken every day at a fixed time. Thus the fixed beginning and ending of observation time could result in underestimation of true maximum events, especially for short daily durations [Perica *et al.*, 2013]. Daily-to-24hour conversion factor was introduced as 1.13. Weighted frequency estimates above were multiplied by 1.13 and 1.04 (grid to point conversion) to find final products: weighted point estimates for 24hour-2year, 5year, 10year, 25year, 50year, 100year events.

### 2.3 Determination of Confidence Intervals for Extreme Events

After applying methods in 2.1 to AMS processed from each climate model realization, we can not only calculate the expected values of extreme precipitation event of different quantiles but also their confidence intervals are available to us. This type of uncertainty comes from the Monte Carlo simulation process which could reflect the parameter uncertainties in distribution curve fitting procedure. To preserve this information, besides expected values, 500 more corresponding data points from simulation were also saved.

In 2.2, weights for each climate model realization were determined in order to get weighted ensemble results of extreme precipitation values. Besides, they are useful to derive weighted

ensemble results of corresponding confidence intervals, noting that uncertainties incorporated in this type of confidence interval include two types: climate model uncertainty as well as sampling uncertainty (parameter uncertainty). Thus it is a broader and more robust description compared to confidence intervals described in Atlas 14, and it should be provided as a more reliable design reference for municipal facilities in the future.

The key idea to calculate weighted confidence intervals is very simple: fitting a distribution curve to data points. Take 100 year-24 hour precipitation event as an example, suppose we have 30 model realizations, each realization has different weights and the corresponding weight are assigned evenly to 500 data points within each realization. One may naturally calculate weighted traditional moments and then use these moments statistics to calculate distribution parameters. Weighted mean, variance, and skewness can be calculated with the formula given by [Rimoldini, 2013]. However there are two major deficiencies. Firstly, as mentioned earlier, traditional moments are not as robust as L-moments to sample errors, since error will propagate non-linearly, thus fitted curve may be largely biased. Secondly, for certain types of distributions, parameters have no explicit form in terms of traditional moments or the explicit form is too complicated. Therefore, we decided to construct new data series based on data points and weights in different climate model realizations and then calculated L-moment statistics of the new data series. Finally, we were able to fit different curves based on L-moment ratios and found best-fit distribution to provide weighted confidence intervals.

## Chapter 3 Weighted Ensemble Analysis and Uncertainty Assessment

In chapter 2, we discussed methods of using regional frequency analysis to derive rainfall event values for each model and using tricube function to assign weights for the model ensemble. Additionally, a new method based on Monte Carlo simulation was implemented to analyze the confidence intervals for event values. In this chapter, the whole methodology is applied to our study region to provide expected values and confidence intervals for 24-hour rainfall under different recurrence intervals and different climate scenarios, for both historical period and future horizon. These results will be later compared with some current available results from different research institute.

### 3.1 Determination of Extreme Event Values for Future

#### 3.1.1 Calculation of Historical Extreme Event Values

As mentioned in chapter 2, it is crucial to partition sites into different homogenous regions, in which the frequency distribution of sites are identical apart from the site-specific scaling factor [Jonathan Richard Morley Hosking and Wallis, 2005]. In this study, considering our study region is not considerably large, instead of partitioning from pre-selected sites, we treated pre-selected sites as one single region at the first stage. With the available AMS observation data of daily precipitation, we use discordancy and heterogeneity tests to eliminate those sites that cannot pass the test, and then we re-test the new region to see whether all remaining sites should be treated as one homogenous region. The ultimately selected sites (17 in total) for this study are shown in Figure 4 and listed in table 2, including 12 stations from NOAA-NCDC network and 5

stations from ISWS-CCPN network.

After determining the site combination based on observation dataset, we extracted the AMS model data of daily precipitation data from different cells corresponding to our site selection. There are 40 years of data (1961-2000) in total for 39 model realizations (13 models, 3 realizations per each model). We used these model data to perform RFA to obtain model rainfall event values. Two issues should be noticed in this RFA 1) if one particular model run cannot pass discordancy or heterogeneity test, this model run will not be involved in weighting procedures, thus only 32 of 39 realizations were selected as candidates in weight determination procedure. 2) Spatial correlation among sites was also considered in this analysis, coefficients of correlation of AMS between different sites were calculated and the mean value was chosen as correlation parameter in regional frequency analysis. By comparing model rainfall event values and observation rainfall event values calculated from same location and same period, weights for different models is determined in the next step.

### 3.1.2 Determination of Weights for Model Ensemble

Before weight determination procedures, extreme event values calculated from observation dataset were multiplied by 0.96 to account for point-to-grid conversion; following that observation results and model results were compared under the same scale to calculate weights for models. The weighting procedure was based on the following idea: assessing the model deviation from observation results, if the deviation for one model is greater than the threshold, weight for that model should be 0; if one model outperforms other models, more weight should

be assigned for that model. An arithmetic form was described in chapter 2 as the tricube weight function defined by [Mosteller and Tukey, 1977]. Percentage departures of each model realization from observation (averaged over P2-P100 events) are plotted in Figure 6 and Figure 7.

From figure we can conclude: a) model performance varies from “over-estimate all sites” to “under-estimate all sites”, but there are still plenty of model realizations that could provide “unbiased estimate across all sites”. b) for each of the study sites, model realization ensemble could cover the “true value” and provide a unbiased range. Followed by the percentage departure information, weights for different model realizations were calculated from the tricube weight function and then rescaled from 0 to 1, Noting that only 3 realizations are available per each model due to data availability, they may not be enough to cover the whole possible range of model simulation. To avoid over-weighting for particular model realization, weights for a particular model were firstly sum up and then evenly distributed to its realizations. Weighting results of model realizations are shown in Figure 8.

### 3.1.3 Extreme Event Values for Future

Similarly, extreme event values of different models are calculated by regional frequency analysis based on two future periods: 2046-2065 and 2081-2100, under three CMIP3 climate scenarios: A1B, A2 and B1. Providing weights for different model realizations derived in previous step, weighted extreme event values were calculated in two future periods under different climate change scenarios. This type of results could serve as a reference for future municipal facility

design as well as runoff generation analysis. A full list of estimate values for both historical and future periods are shown in Table 5 to Table 12.

As shown in Figure 9, we have two major findings regarding the temporal change of precipitation events. Firstly, under all emission scenarios (A1B, A2 and B1) and all recurrence intervals (P2-P100), precipitation quantiles increase significantly from historical period to 2050s; they continue to increase slightly from 2050s to 2100s. This phenomenon suggests that the first 50-year period of this century is crucial to mitigating the climate change impact, and immediate policies or activities should be implemented to control the more frequent extreme precipitation and the resulting floods. Secondly, if we compare precipitation quantiles between different emission scenarios, we are able to find that in 2050s, quantile values are the highest under scenario A1B, followed by A2 and B1. During 2100s, things change a little bit, and quantile values are the highest under scenario B1, followed by A1B and A2. However the difference between B1 and A1B is quite small. If we recall the description of different emission scenarios, it is surprising that technology development and resource-efficient production cannot offset the impact of rapid economic growth on more frequent extreme events. Since we cannot simply slow down economic growth to mitigate its impacts on climate, a more proper way would be increasing the investment for municipal facility upgrade to enhance its reliability against increasing and more frequent precipitation and flood events. In addition to site average results, a group of isoheytal maps reflecting spatial distribution of extreme precipitation events are also shown in Figure 10 to Figure 15.

## **3.2 Determination of Confidence Intervals**

### **3.2.1 Description of Confidence Intervals and Sources of Uncertainties**

Our best estimates of the precipitation event values are the weighted mean results based on model ensemble. However, the method does not provide the level of confidence in these estimates. Confidence intervals (CI) are introduced to quantify the level of confidence, which are a measure of uncertainty of these estimates. CI reports two values, the upper confidence limit (UCL) and the lower confidence limit (LCL), between which the true value of the precipitation quantile would lie under certain CI. For example, if the confidence level is 90 percent, we are 90 percent sure that the true value for the precipitation quantile is between these CLs. There are two properties of the CI : a) The higher the CL, the wider the confidence intervals; b) UCL and LCL are not necessarily equidistant from the estimates, since the distribution to determine CI can be skewed.

Two different sources of uncertainties are included in this study, namely model variability and sampling variability. The final estimate is expressed as weighted ensemble of model results. Each model result can be regarded as one “observation” for precipitation estimate with particular weights, thus model ensemble could provide us a range of “true estimates” and that is why model variability exists. In terms of sampling variability, it is a concept regarding single model. As described in Chapter 2, during the curve-fitting procedure in determining estimates for different recurrence intervals, our selected distribution will never be a perfect proxy and the distribution parameter uncertainty is inherent. Also, given data availability for historical



observation for only 40 years, uncertainty of estimates increases as recurrence interval increases. Thus in regional frequency procedure, besides expected values for particular events, 500 more data points from Monte Carlo simulation are also reported [*J. R. M. Hosking, 2015*], which can be used as a good proxy to reflect sampling variability. Figure 16 displays Monte Carlo simulation results from each model realization. We can find that for larger value of recurrence intervals, the range of simulated value over expected value becomes wider, which means greater uncertainties are brought forward. This is reasonable since given limited length of AMS, for example 40 years of data, 10-yr event calculated from 40 years of data will be more reliable than 100-yr event calculated from same time series.

### 3.2.2 Weighted Confidence Intervals Reflecting Model Variability

Since we already have results of weight ensemble for corresponding models as well as precipitation estimates from different models for different recurrence intervals at each site, the next step is to utilize these results to derive confidence intervals. Firstly, we would only consider model variability for simplicity and then add sampling variability in the following part.

Take 100-year event in 2050s at O'hare Airport Station as example, the key idea is to fit a distribution to estimate results from different models, however the tricky part is that each result has its own weights. It is possible to calculate weighted statistical moments (mean, standard deviation, skewness), however, with traditional higher order moments results, it is hard to derive parameters in some 3-parameter distributions which are used as our candidates.

Since the analytical solution for parameters is either too complicated or does not exist under a

moment method. Therefore, we decide to generate a proxy data series and use L-moments to fit curves and calculate CI.

Define  $X_i$  as estimate result from  $i^{\text{th}}$  model,  $w_i$  is the corresponding weight, first we can multiply  $w_i$  by 1000 (for example) and round it, denote the new number as  $W_i$ . Second, each  $X_i$  can be repeated  $W_i$  times to generate a new series  $S$  altogether,  $S$  could reflect the distribution of estimate results. Afterwards, L-moment statistics can be calculated for  $S$  and based on such statistics, we can fit some 3-parameter distribution to  $S$  and finally, find the best fit curve to get CI. These procedures are processed with R language using ImomRFA package [J. R. M. Hosking, 2015].

### 3.2.3 Weighted Confidence Intervals Reflecting Model and Sampling Variability

As mentioned in section 3.2.1, in order to get a more robust estimate of CI, sampling variability in an important source of prediction uncertainty and cannot be neglected. Followed by the idea described in 3.2.2, for the  $i^{\text{th}}$  model, 500 data points from Monte-Carlo simulation should also be repeated  $W_i$  times, in addition to estimate result (expected value) to generate new series  $S$ . After the new series is generated, similar calculation procedures are applied as in 3.2.2.

Results are shown in Figure 17 to Figure 22 and a whole list of CIs of different recurrence intervals and emission scenarios for each sites are shown in Table 13 to Table 18. Take 100-year and 2-year events as example, the results are similar to changes of expected values. When averaged over all sites, confidence intervals increase significantly from historical period to 2050s, increase slightly from 2050s to 2100s. Under most emission scenarios in both 2050s and 2100s

(except 100-year and 50-year events under A2 scenario in 2100s), confidence intervals are the narrowest under A2 scenario compared to A1B and B1 scenario, while the latter two have comparable CI width. If the worst cases are considered, i.e. upper confidence interval, we have the following findings. During the 2050's, upper CI is the largest under A1B scenario and the lowest under A2 scenario. However in 2100s, upper CIs under A1B and A2 scenario are comparable and the latter is even greater for 100-year and 50-year events. A2 describes a very heterogeneous world where population growth is high but technology changes are slower compared to other storylines, this variability at the social side might be one reason for uncertainty in the prediction of extreme precipitation events.

### **3.3 Comparison between two types of Confidence Intervals**

Section 3.2.2 and 3.2.3 defined two types of confidence intervals: model variability (sample variability, type I) and parameter variability (sampling variability). Naturally we may conjecture that adding parameter variability into consideration will bring wider confidence intervals of precipitation quantile estimates. In this study, historical model simulation data (1961-2000) were analyzed to prove the aforementioned argument. Results are displayed in Figure 23 to Figure 28. From 2-year to 100-year events, adding parameter variability (type II) provides wider confidence intervals the larger recurrence interval is, the wider confidence intervals are. Averagely, type II confidence interval is 24.9%, 34.0%, 36.6%, 18.0%, 4.0%, 6.1% wider than type I confidence interval.

### **3.4 Research Results vs NOAA Atlas 14 results**

NOAA Atlas 14 (Volume 2) was released in 2004 and revised in 2006; it provided precipitation frequency estimates from 5-minute to 60-day durations with recurrence intervals of 1-year to 1000-year; the associated confidence intervals were also reported. The study region of Volume 2 included Delaware, District of Columbia, Illinois, Indiana, Kentucky, Maryland, New Jersey, North Carolina, Ohio, Pennsylvania, South Carolina, Tennessee, Virginia and West Virginia [Perica et al., 2013]. Similar to our study, it applied regional frequency analysis based on L-moments [Jonathan Richard Morley Hosking and Wallis, 2005] and was based on annual maximum series of observed precipitation. However, the sites of interest as well as record length are different from our study and the reported confidence intervals only took parameter variability into consideration. By comparing two groups of results, we may observe the potential to update current design rainfall standard in the future, this study could serve as justification for managers to adopt more stringent and conservative standards in urban flood protection facility design [Hennegriff, 2007].

#### 3.4.1 Comparison of expected values

After averaging over 17 sites, in historical period, weighted model ensemble prediction is 6.7% lower compared to Atlas 14 result for 100-year event, whereas 9.0% higher for 2-year event. In 2050s, this percent change goes to 15.8% (A1B), 10.2% (A2), 3.6% (B1) for 100-year event and 21.6% (A1B), 18.6% (A2), 17.4% (B1) for 2-year event. In 2100s, this percent change goes to 15.6% (A1B), 13.5% (A2), 16.5% (B1) for 100-year event and 26.5% (A1B), 22.6% (A2), 26.4% (B1) for 2-year event. Spatial patterns are shown in Figure 29 to Figure 32.

### 3.4.2 Comparison of confidence intervals

In the comparison of confidence intervals, only the worst condition, the upper confidence intervals, is considered. Atlas 14 and this study both report 90% confidence intervals. Since a more comprehensive description of sources of uncertainty was introduced in this study and the essential property that future condition is more uncertain compared to historical estimates, our study provides much greater confidence intervals. Taking 100-year event as an example, during 2050s, confidence intervals are at least 20% higher (in A2 scenario) and can go up to 67.6%. By average, confidence intervals are 30%-40% higher under three emission scenarios. In 2100s, confidence intervals become wider but compared to 2050s, the difference is not significant. The only exception is A2 scenario. In 2050s, it is 20%-50.6% higher than Atlas 14 while in 2100s, it dramatically goes up to 40.5%-87.1%. Spatial patterns of 100-year and 2-year events are shown in Figure 33 to Figure 36.

## Chapter 4 Weighted Ensemble Analysis Based on Maximum Entropy

### Method

In chapter 3, tricube weighting function was applied in weighted ensemble analysis to find expected values and confidence intervals for 24-hour rainfall under different recurrence intervals and different climate scenarios, for both historical and future periods. This type of weight determination procedure more or less relies on the stationary assumption: i.e., “good performance” of a climate model during the past will “remain good” in the future. Since we do not have information regarding the distribution pattern of precipitation events in the future, one may naturally argue that the performance of climate model will change with time. Therefore in this chapter, a method dealing with limited prior data, namely maximum entropy method (MEM), is introduced and applied for weight determination [Laurent and Cai, 2007]. Expected values of quantiles are calculated with new weight ensemble and are compared with results from chapter 3.

#### 4.1 Introduction of MEM

After the definition of thermodynamic entropy by Boltzmann, Shannon defined information entropy in 1947, which describes the expected value of the information contained in the flow of information [Shannon, 2001]. The entropy of certain distribution is defined as follows

$$H(p) = - \sum_{i=1}^N p_i * \ln (p_i) \quad (4.1)$$

where  $p=(p_i)$  is the probability distribution and the entropy could measure the uncertainty of this distribution. Entropy is inversely proportional to the uncertainty.

Given a method of determining probability distribution, its corresponding entropy is able to measure how close this method is to the “true way” (Laurent and Cai). As described in Laplace’s Principle of Insufficient Reason, if we do not have enough information to justify condition A more than condition B, then the only reasonable way to describe this knowledge is to assign equal probabilities to both conditions [De Fraiture, 2003] . Under this condition, the entropy reaches maximum under uniform distribution condition. If entropy is going to be maximized under constraints, the resulting probability distribution is determined under “true way” hypothesis as well as constraints to reflect available information. This idea was firstly raised by Jaynes in 1978 as an extension of Laplace’s Principle of Insufficient Reason, namely maximum entropy principle (MEP) [Jaynes, 1978].

MEM could help solve problems under incomplete information, just as described in our study where future prediction reliability of different models is not available. Unknown variables will be written in probability form and available information will serve as constraints, which in this study is the model performance based on historical observation. Therefore, an optimization model is described in 4.2 to optimize  $H(p)$ .

#### **4.2 Determination of Weights for Model Ensemble with MEM**

[Laurent and Cai, 2007] has applied MEM to combining general circulation models (GCMs) for regional climate change assessment. In the process of entropy maximization, error terms between combined GCM results and observation results were included as constraints, upper and lower limits were parameters to constrain errors. Similar ideas were adopted in this study

and the formulation of optimization model is described as follows

$$\text{Maximize } H = \sum_{i=1}^N w_i \ln(w_i) - \sum_{j=1}^{17} [q_j \ln(q_j) + (1 - q_j) \ln(1 - q_j)] \quad (4.2)$$

$$S.T. O_j = \sum_{i=1}^N w_i M_{i,j} + q_j V + (1 - q_j)(-V), j = 1, 2, \dots, 17; \quad (4.3)$$

$$\sum_{i=1}^N w_i = 1; \quad (4.4)$$

$$w_i \in [0, 1]; q_j \in [0, 1]; \quad (4.5)$$

where  $i$  represents the loop of climate model realizations,  $j$  represents the loop of sites.  $O_j$  is the precipitation quantile calculated from observation data for site  $j$  while  $M_{i,j}$  is the precipitation quantile calculated from model realization  $i$  for site  $j$ .  $w_i$  and  $q_j$  are decision variables,  $w_i$  is the weight for model realization  $i$ ,  $q_j$  is related to error terms after adding them to weighted ensemble framework

$$O_j = \sum_{i=1}^N w_i M_{i,j} + e_j, j = 1, 2, \dots, 17; \quad (4.6)$$

Where  $e_j$  is the error between weighted ensemble and observation results. Suppose the error is not skewed and is centered at 0,  $-V$  and  $V$  are lower and upper bounds for error respectively, therefore  $e_j$  can be expressed as linear combination of bounds with discrete probability distribution ( $q_j, 1-q_j$ )

$$e_j = q_j V + (1 - q_j)(-V), j = 1, 2, \dots, 17; \quad (4.7)$$

The entropy corresponding to this discrete distribution is

$$H = -q_j \ln(q_j) - (1 - q_j) \ln(1 - q_j) \quad (4.8)$$

Therefore, the objective function in the optimization model can be treated as a combination of entropy for weight distribution and entropy for error distribution. Maximizing entropy for



weight distribution will assign equal weights to each model realization result while minimize error terms will serve as constraints, as mentioned in the maximum entropy principle.  $V$ , the error bound, is an artificial parameter. In this study,  $V$  was selected as 10mm, 5mm and 2mm for comparison. Only 100-year events were analyzed and compared. The optimization model was programmed and solved in GAMS (General Algebraic Modeling Systems) [Rosenthal, 2008].

#### **4.3 Expected Values of Quantiles: Results and Comparison**

After we run the optimization with different  $V$  values, different weight ensemble results are shown in Figure 37 to Figure 39.

First, compared to weighted ensemble method based on tricube weight functions shown in Figure 40, MEM assigns weights for a smaller number of model realizations under stricter error constraints ( $V=2$ ,  $V=5$ ). Second, as  $V$  increases, more model realizations are assigned certain weights. This is reasonable since if  $V$  is large, the error constraints are released and the optimization model tend to only maximize the entropy from the weight distribution. As mentioned earlier, this will tend to assign equal weights to all model realizations. Third, if we focus the model realization with best performance, i.e. the highest weight,  $er\_3$  is the best from MEM, which is consistent with weighted ensemble method. When  $V=2$  and  $V=5$ , the highest weight is nearly 0.5; however if  $V$  continues to increase, its weight decreases and goes close to weight result in weighted ensemble method. We also should notice that this weight is not inversely proportional to  $V$ . This results from this study are consistent with those from [Laurent and Cai, 2007].

After weight determination, results were applied to corresponding model realization quantiles, and compared to observation quantiles as well as quantiles from weighted ensemble method, as listed in Table 19.

Apparently, MEM results are very close to WEM results, and they are both able to provide acceptable quantile estimates compared to quantile estimates from observation data. Additionally, we calculated average percentage error of the two methods. The results are: -0.97% (WEM), -1.50% (MEM,  $V=2$ ), 0.91% (MEM,  $V=5$ ), 0.73% (MEM,  $V=10$ ). To our surprise, the performance of MEM is negatively correlated to  $V$  values, i.e. if we release the error bound constraints, the overall performance of quantile estimate will be better. If  $V$  is very large, MEM tend to assign equal weights for all model realizations, which converges to the arithmetic mean of model ensemble. This may suggest at least, taking average value of model ensemble to estimate quantiles will perform no worse than complicated methods such as weighting approaches. It can even provide better performance with less computational work in our case. However, we cannot justify the better performance in determining confidence intervals, which needs further research.

## Chapter 5 Conclusions

This study uses observed daily rainfall data from NCDC and CCPN network as well as statistical downscaled daily rainfall data from 13 GCMs in both historical period (1961-2000) and future period (2046-2065 and 2081-2100) under 3 CMIP3 emission scenarios (A1B, A2 and B1). The area of interest is Chicago area (Cook County, Illinois). Regional frequency analysis was adapted to get 24-hour extreme precipitation quantiles with different recurrence intervals: 2-year, 5-year, 10-year, 25-year, 50-year and 100-year. By comparing historical performance of different climate models against observation results, corresponding weights were assigned to different model realizations through weighted ensemble method (WEM) and maximum entropy method (MEM). Then, these weight results were applied to projected precipitation quantiles to calculate weighted quantile estimates in the future. Additionally, in order to measure the uncertainty of these estimates, based on Monte Carlo simulation, a new approach which could combine model uncertainty and parameter uncertainty was adopted to provide robust confidence intervals. These results were interpreted both in values and isoheytal maps and further compared with current available results from NOAA Atlas 14. Finally, the estimation performance and parameter sensitivity of MEM were also assessed and discussed.

### 5.1 Findings

Under all emission scenarios (A1B, A2 and B1) and all recurrence intervals (P2-P100), precipitation quantiles increase significantly from historical period to 2050s; they continue to increase slightly from 2050s to 2100s. This phenomenon suggests that the first 50-year period

of this century is crucial to mitigating the climate change impact, and immediate policies or activities should be implemented to control the more frequent extreme precipitation and the resulting floods.

In 2050s, quantile values are the highest under scenario A1B, followed by A2 and B1. During 2100s, things change a little bit, and quantile values are the highest under scenario B1, followed by A1B and A2. However the difference between B1 and A1B is quite small. If we recall the description of different emission scenarios, it is surprising that technology development and resource-efficient production cannot offset the impact of rapid economic growth on more frequent extreme events. One possible way to solve this issue would be increasing the investment for municipal facility upgrade to enhance its reliability against increasing and more frequent precipitation and flood events.

As for the temporal change patterns of confidence intervals, take 100-year and 2-year events as example, the results are similar to changes of expected values. When averaged over all sites, confidence intervals increase significantly from historical period to 2050s, increase slightly from 2050s to 2100s. Under most emission scenarios in both 2050s and 2100s (except 100-year and 50-year events under A2 scenario in 2100s), confidence intervals are the narrowest under A2 scenario compared to A1B and B1 scenario, while the latter two has comparable CI width. If the worst cases are considered, i.e. upper confidence interval, we have the following findings. During the 2050's, upper CI is the largest under A1B scenario and the lowest under A2 scenario. However in 2100s, upper CIs under A1B and A2 scenario are comparable and the latter is even

greater for 100-year and 50-year events. A2 describes a very heterogeneous world where population growth is high but technology changes are slower compared to other storylines, this variability at the social side might be one reason for uncertainty in the prediction of extreme precipitation events.

In the comparison with NOAA Atlas 14 results, after averaging over 17 sites, in historical period, weighted model ensemble prediction is 6.7% lower compared to Atlas 14 result for 100-year event, whereas 9.0% higher for 2-year event. In 2050s, this percent change goes to 15.8% (A1B), 10.2% (A2), 3.6% (B1) for 100-year event and 21.6% (A1B), 18.6% (A2), 17.4% (B1) for 2-year event. . In 2100s, this percent change goes to 15.6% (A1B), 13.5% (A2), 16.5% (B1) for 100-year event and 26.5% (A1B), 22.6% (A2), 26.4% (B1) for 2-year event. In the comparison of confidence intervals, only the worst condition, the upper confidence intervals, is considered. Atlas 14 and this study both report 90% confidence intervals. Since a more comprehensive description of sources of uncertainty was introduced in this study and the essential property that future condition is more uncertain compared to historical estimates, our study provides much greater confidence intervals. Taking 100-year event as an example, during 2050s, confidence intervals are at least 20% higher (in A2 scenario) and can go up to 67.6%. By average, confidence intervals are 30%-40% higher under three emission scenarios. In 2100s, confidence intervals become wider but compared to 2050s, the difference is not significant. The only exception is A2 scenario. In 2050s, it is 20%-50.6% higher than Atlas 14 while in 2100s, it dramatically goes up to 40.5%-87.1%.

MEM assigns weights for a smaller number of model realizations under stricter error constraints ( $V=2$ ,  $V=5$ ). As  $V$  increases, more model realizations are assigned certain weights. This is reasonable since if  $V$  is large, the error constraints are released and the optimization model tend to only maximize the entropy from the weight distribution. As mentioned earlier, this will tend to assign equal weights to all model realizations. MEM estimation results are very close to WEM results, and they are both able to provide acceptable quantile estimates compared to quantile estimates from observation data. The average percentage error of the two methods are: -0.97% (WEM), -1.50% (MEM,  $V=2$ ), 0.91% (MEM,  $V=5$ ), 0.73% (MEM,  $V=10$ ). To our surprise, the performance of MEM is negatively correlated to  $V$  values, i.e. if we release the error bound constraints, the overall performance of quantile estimate will be better. If  $V$  is very large, MEM tend to assign equal weights for all model realizations, which converges to the arithmetic mean of model ensemble. This may suggest at least, taking average value of model ensemble to estimate quantiles will perform no worse than complicated methods such as weighting approaches. It can even provide better performance with less computational work in our case.

## **5.2 Limitations**

Due to data quality, this research used climate data under IPCC AR4 emission scenarios. However, in the latest IPCC report (AR5) , representative concentration pathways (RCPs) were adopted to describe emission scenarios in CMIP5. CMIP5 incorporates newer emission scenarios, and more sophisticated GCMs, thus CMIP5 is becoming the de facto standard for projections [Ray *et al.*, 2008]. Similar analysis that based on unbiased downscaled CMIP5 datasets is needed

and further compared with our CMIP3 results in the future.

Interdependency between climate models is another issue. [Sanderson *et al.*, 2015] argued that the collection of GCM models share duplicated codes, same forcing and validation data which may bring bias in estimation and spurious correlations. More researches are needed on the physical layer of GCM models to draw the “genealogy tree” of climate models, which could help us understand model interdependency.

In the comparison of quantile estimation performance between weighted ensemble method (WEM) and maximum entropy method (MEM), it is interesting that the latter way can also provide accurate results with high computational efficiency. However, in the calculation of confidence intervals, the performance of MEM is not tested in this research. Further analysis is needed to provide comprehensive assessment of MEM.

## Chapter 6 Figures

Figure 1 IPCC CMIP3 emission scenarios (Source: <https://www.ipcc.ch/pdf/special-reports/spm/sres-en.pdf>)

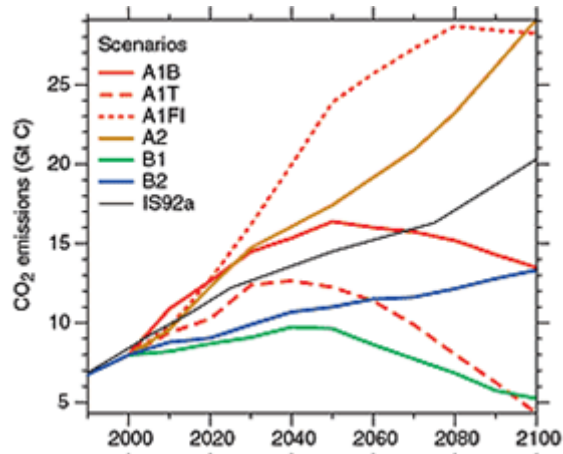


Figure 2 IPCC CMIP5 representative concentration pathways (Source: <https://www.ipcc.ch/pdf/special-reports/spm/sres-en.pdf>)

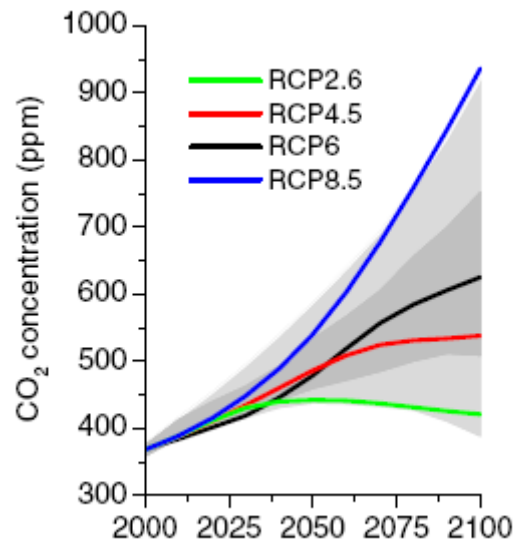




Figure 3 Comparison of SRES and RCP

(Source: <http://www.climatechange.environment.nsw.gov.au/Climate-projections-for-NSW/About-NARCLIM/Emissions-scenarios>)

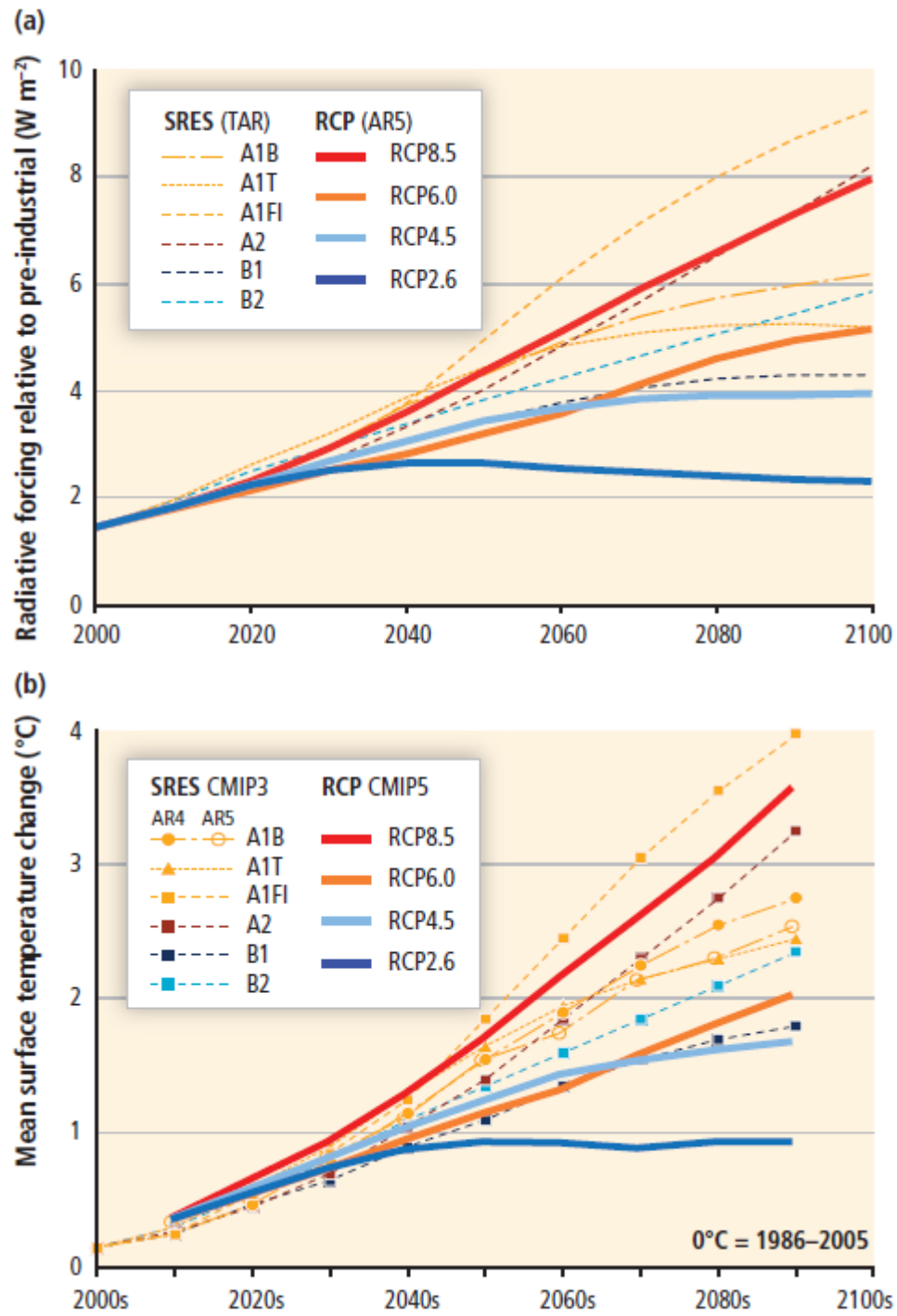


Figure 4 Location of selected stations

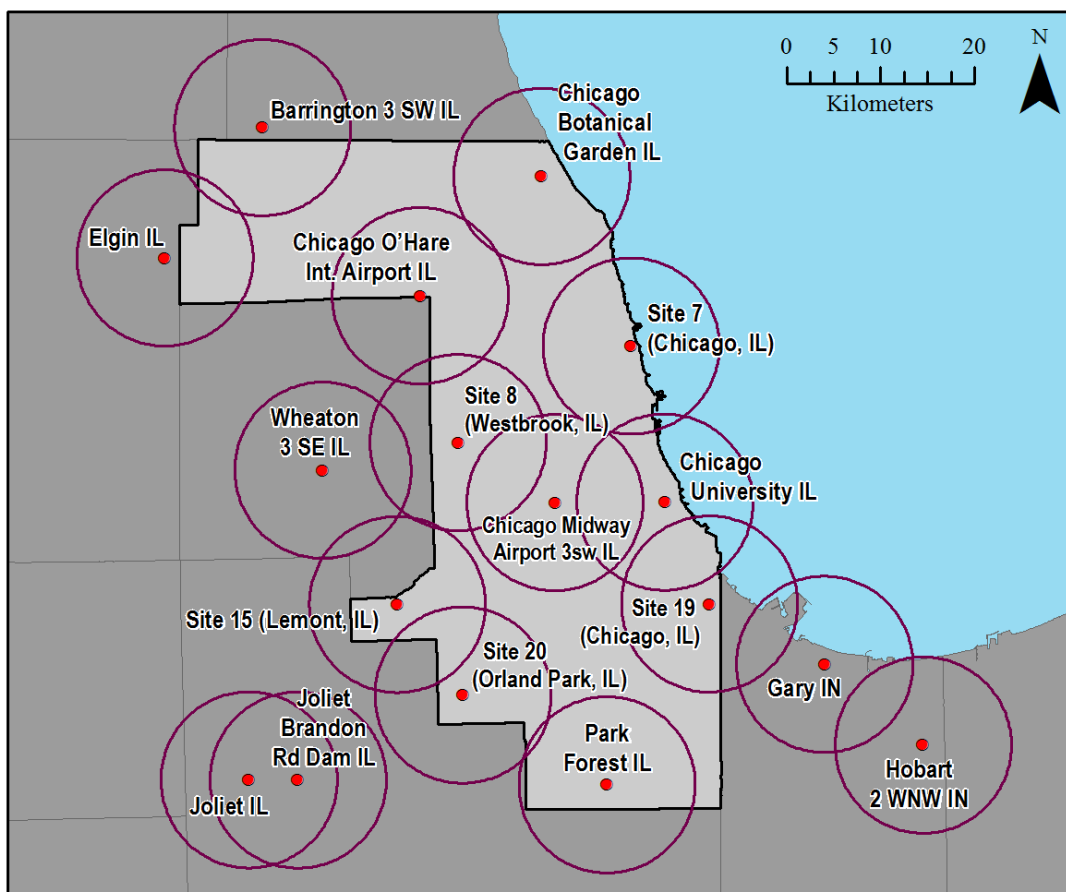


Figure 5 AMS of daily precipitation from dynamical downscaling models (O'hare airport station, 1966-2005)

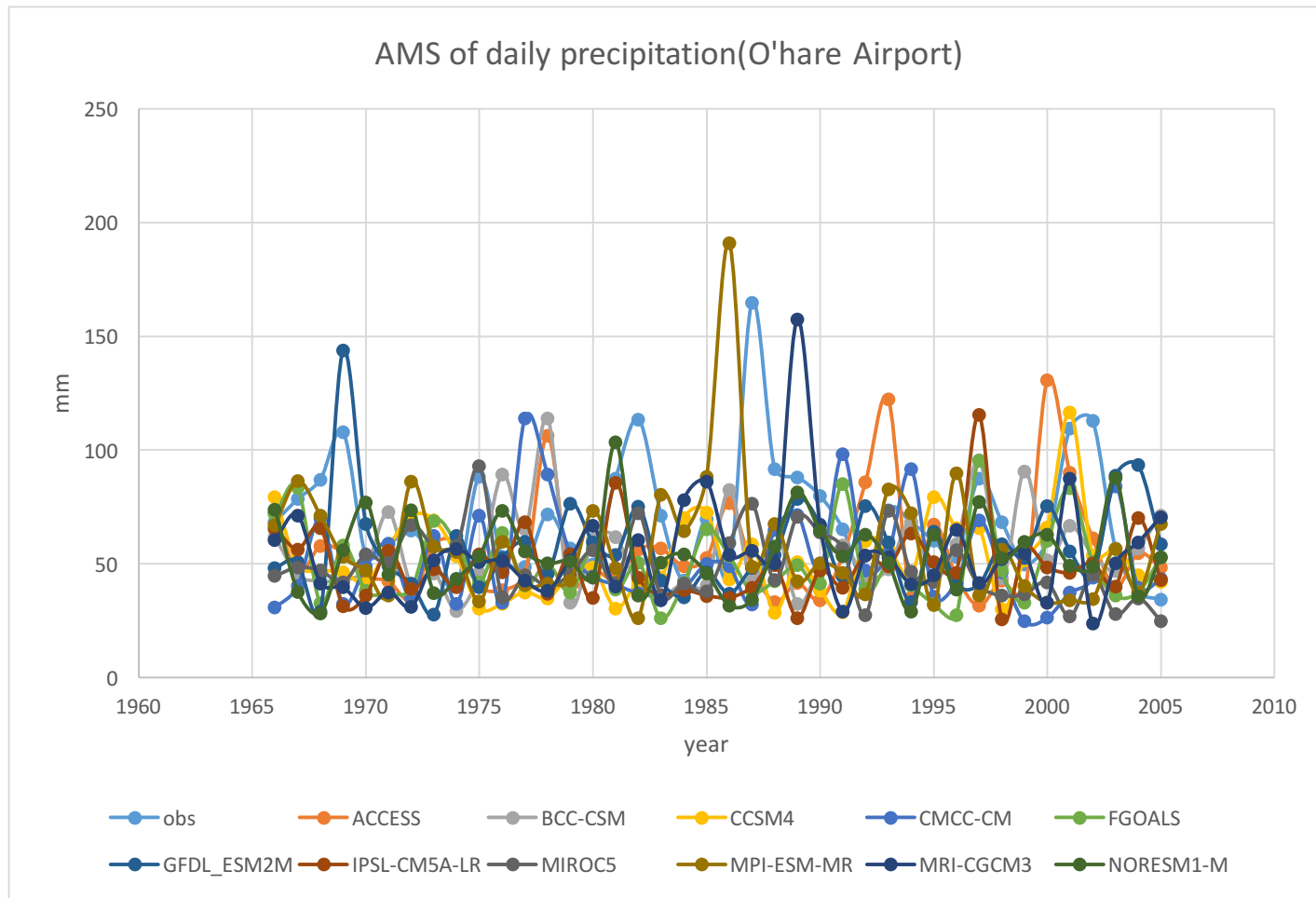


Figure 6 Percentage error of statistical downscaling model estimates (1961-2000)

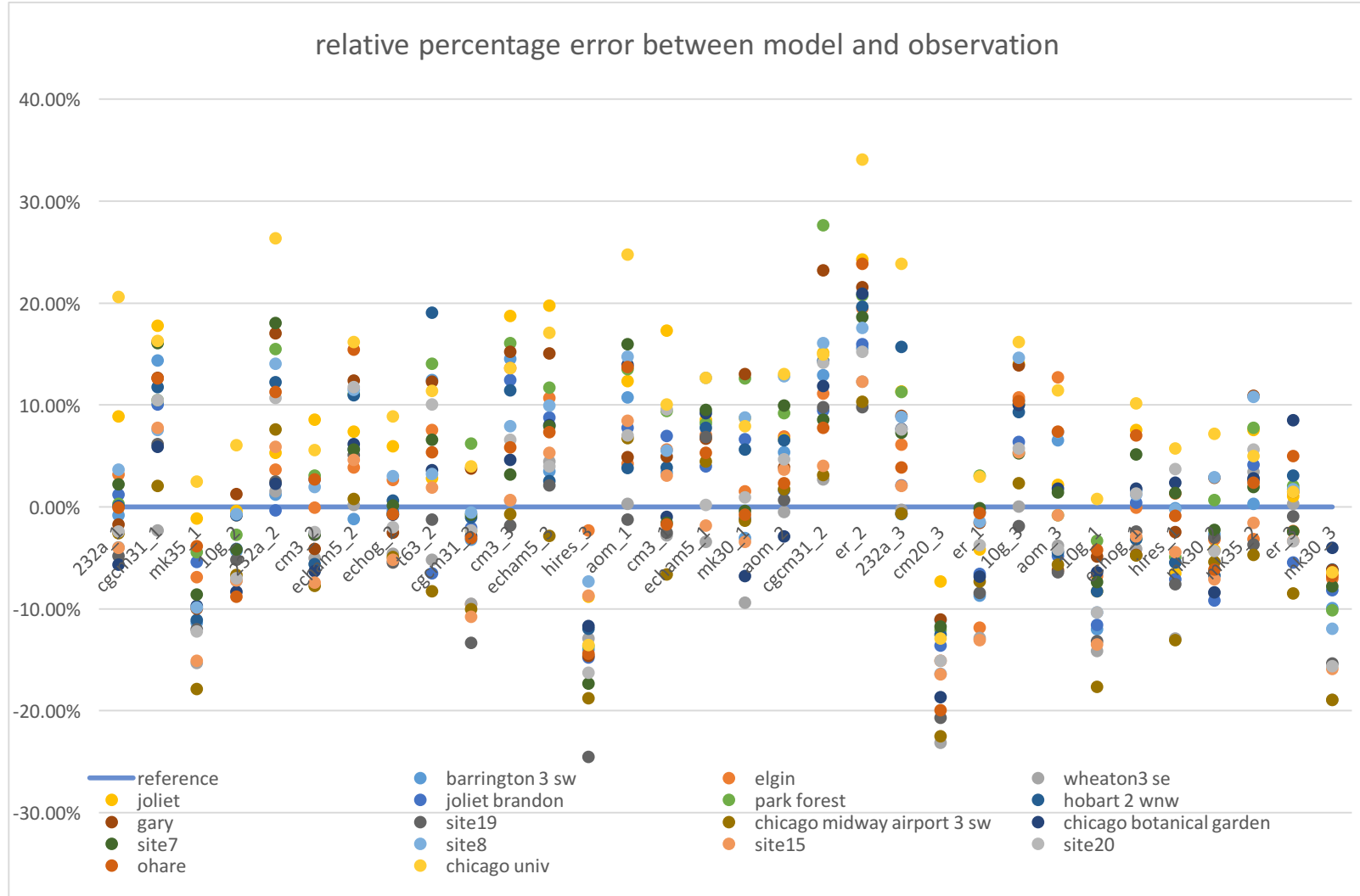


Figure 7 Percentage error of statistical downscaling model estimates (1961-2000)

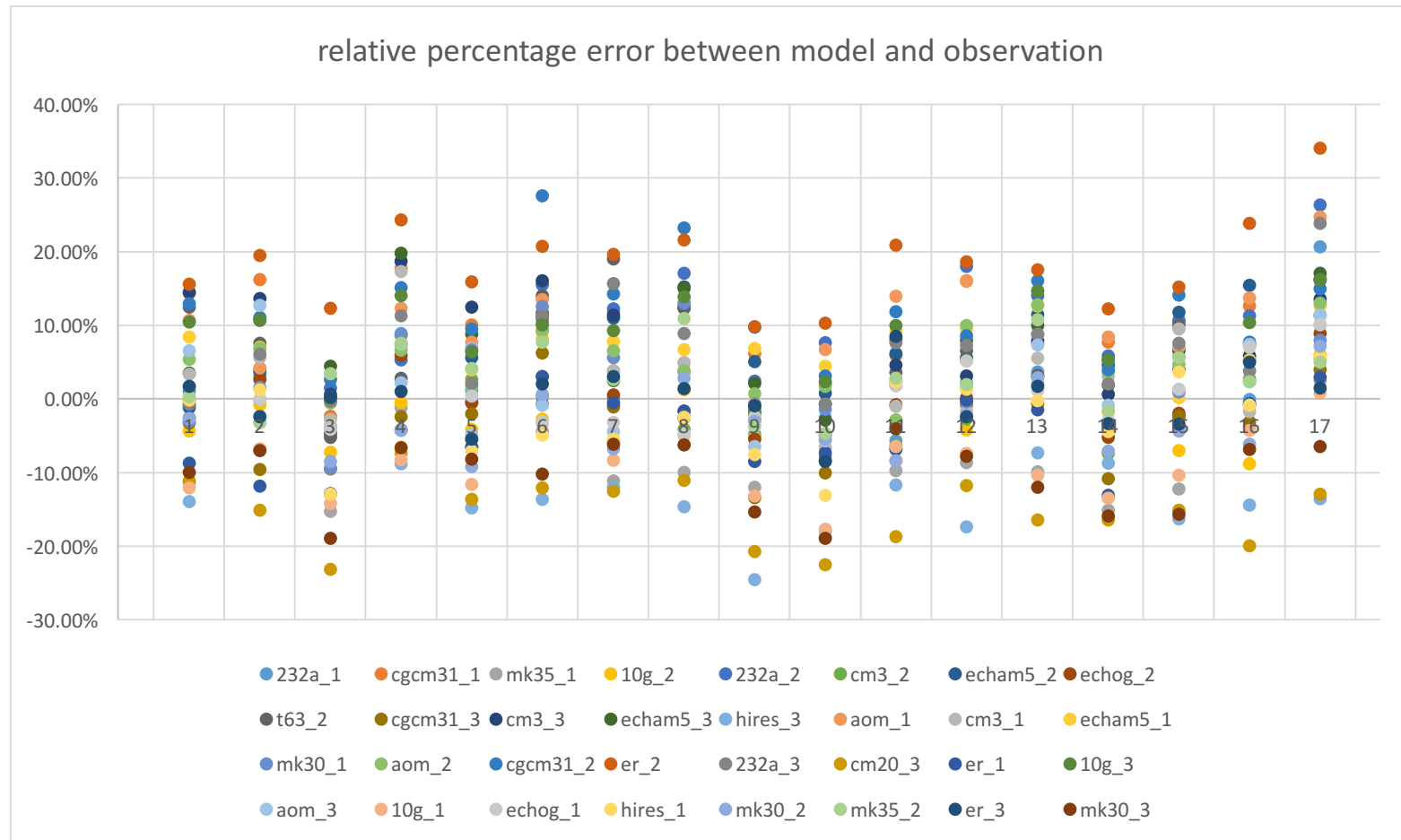


Figure 8 WEM weighting results

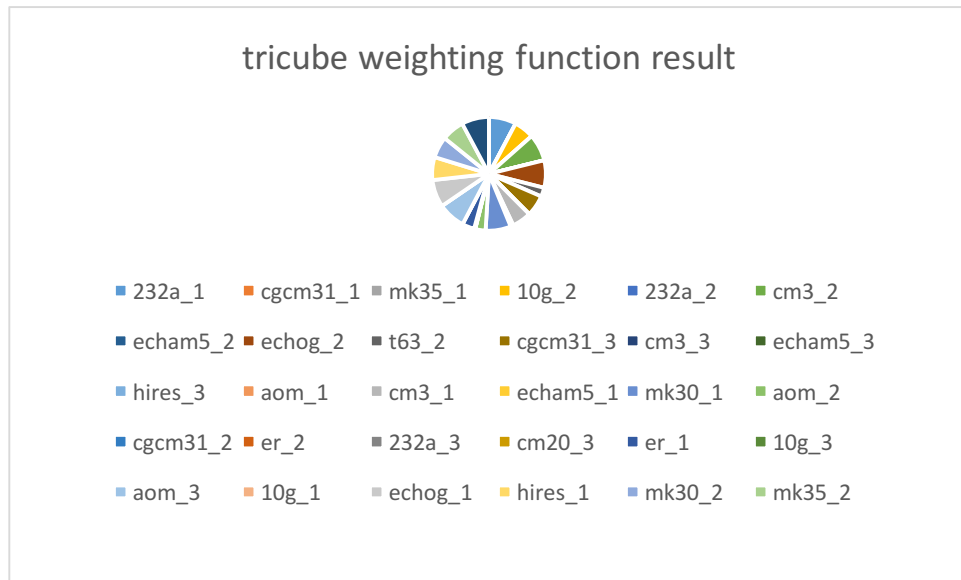


Figure 9 24-hour precipitation event estimates from WEM (site average)

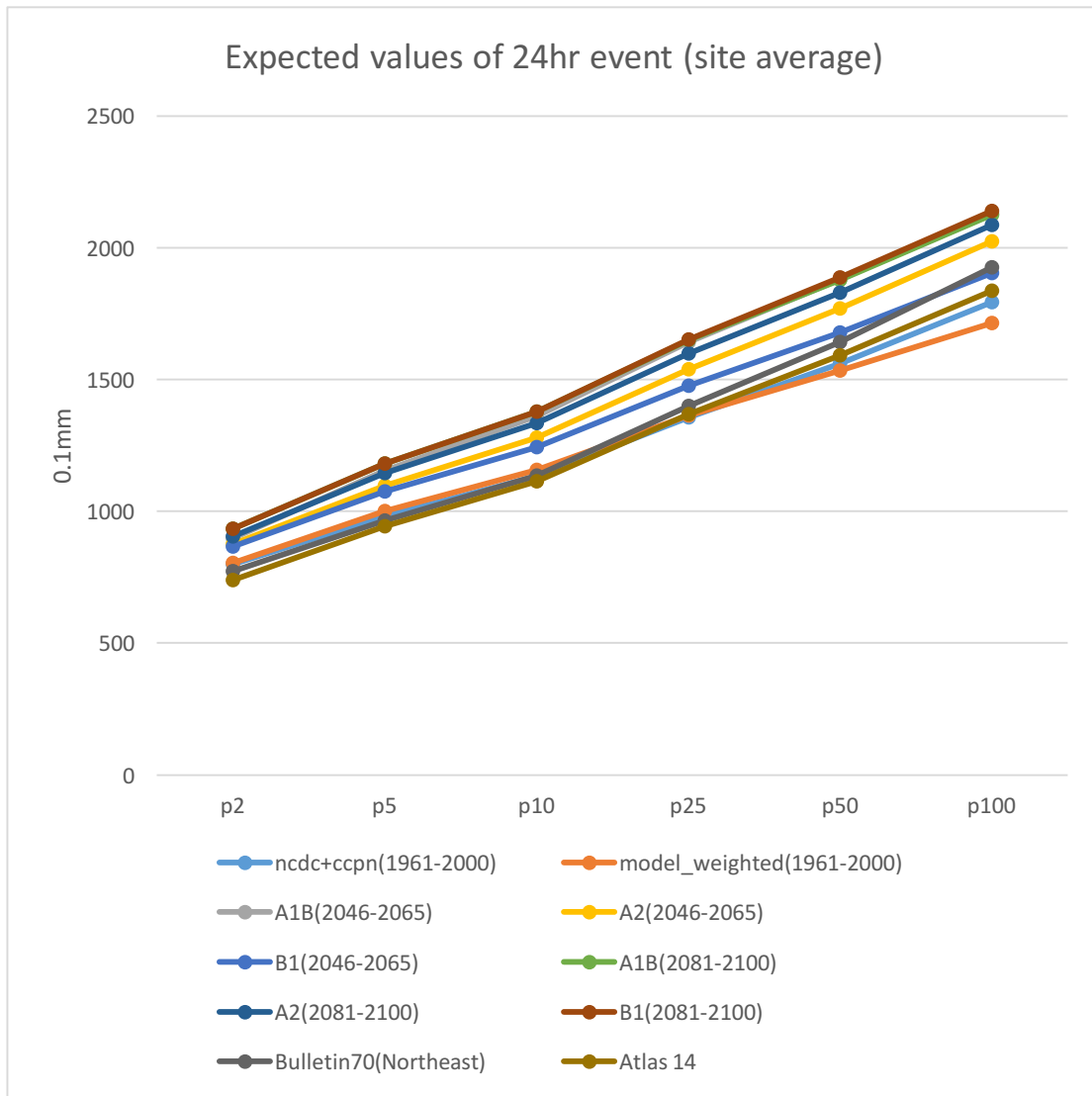


Figure 10 Isohyets for projected 2-year 24-hour precipitation events

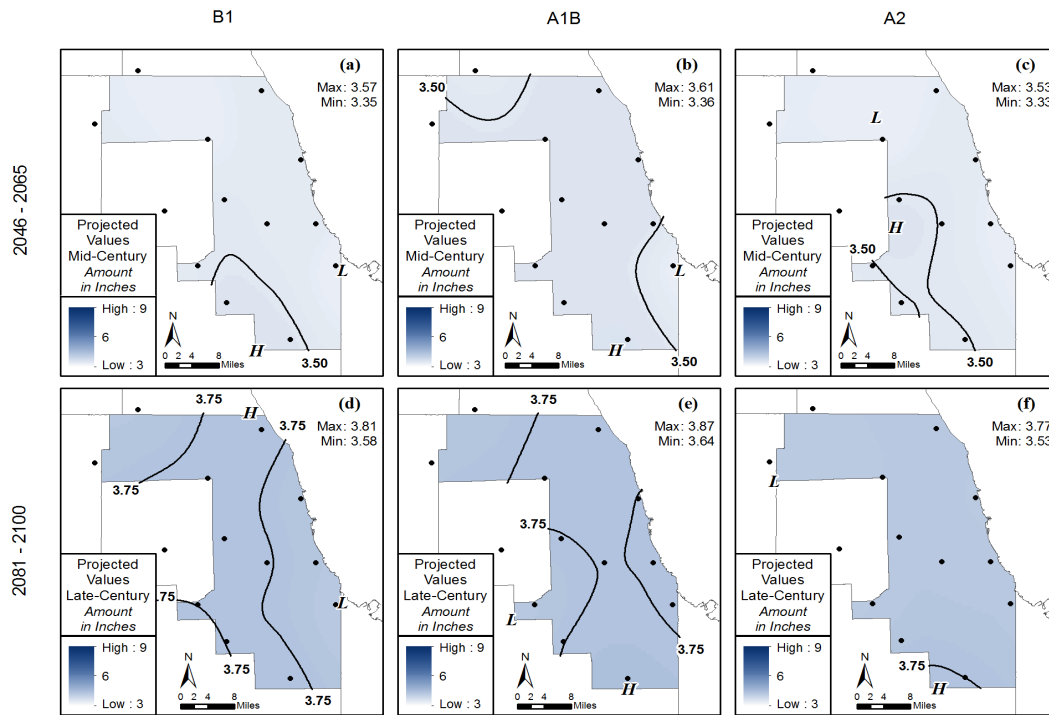


Figure 11 Isohyets for projected 5-year 24-hour precipitation events

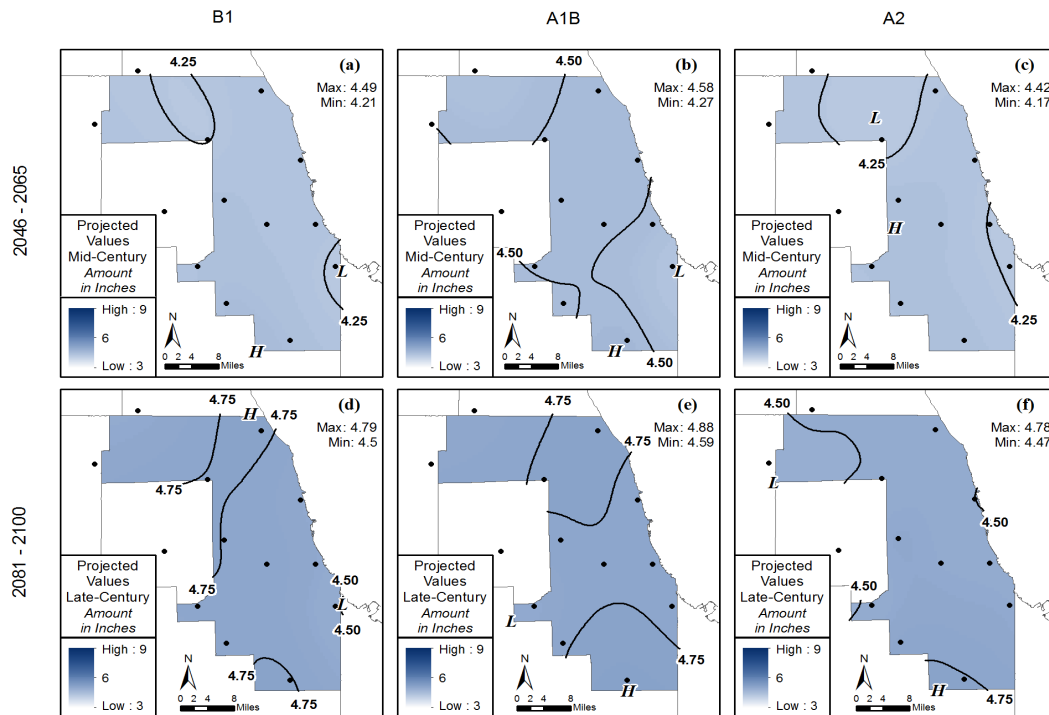




Figure 12 Isoheytals for projected 10-year 24-hour precipitation events

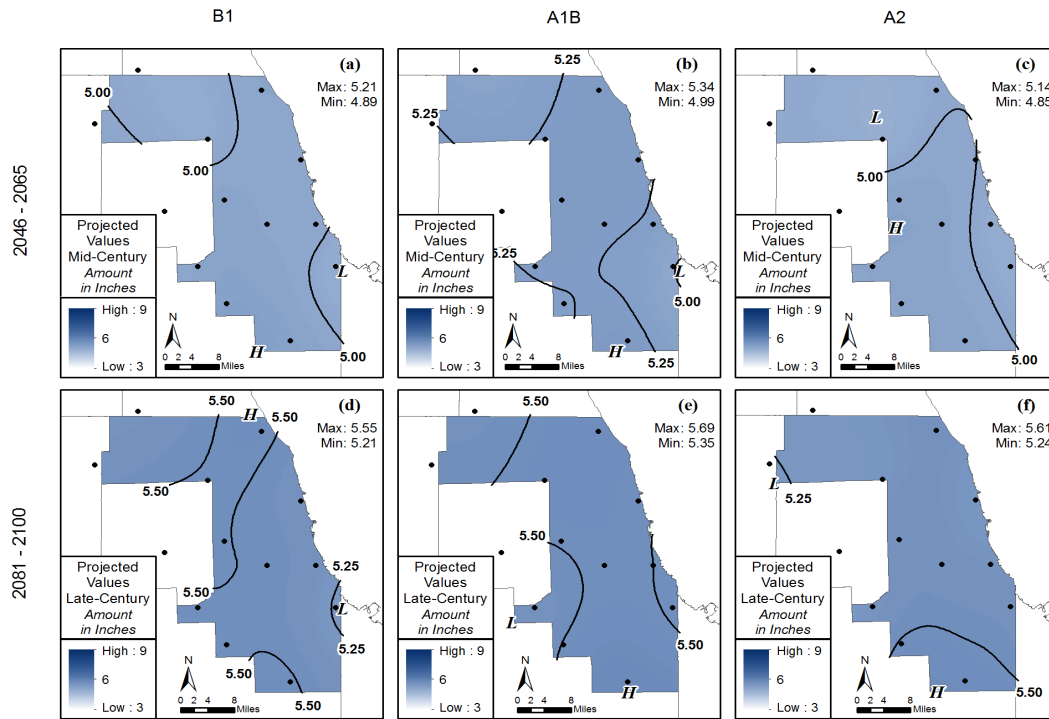


Figure 13 Isoheytals for projected 25-year 24-hour precipitation events

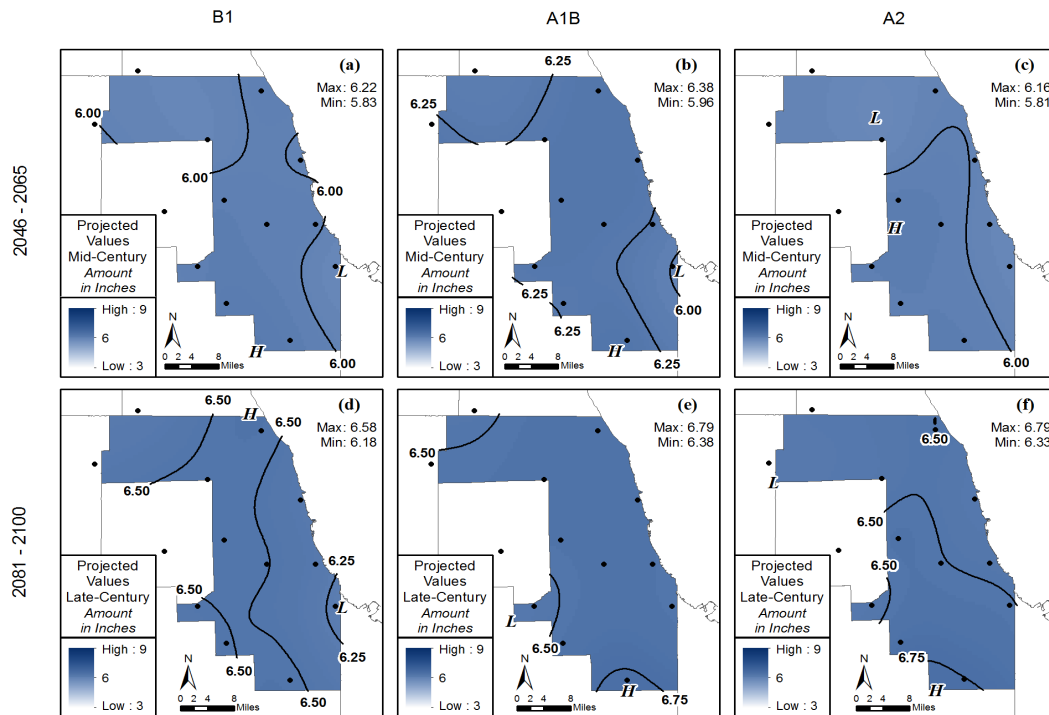


Figure 14 Isohyetals for projected 50-year 24-hour precipitation events

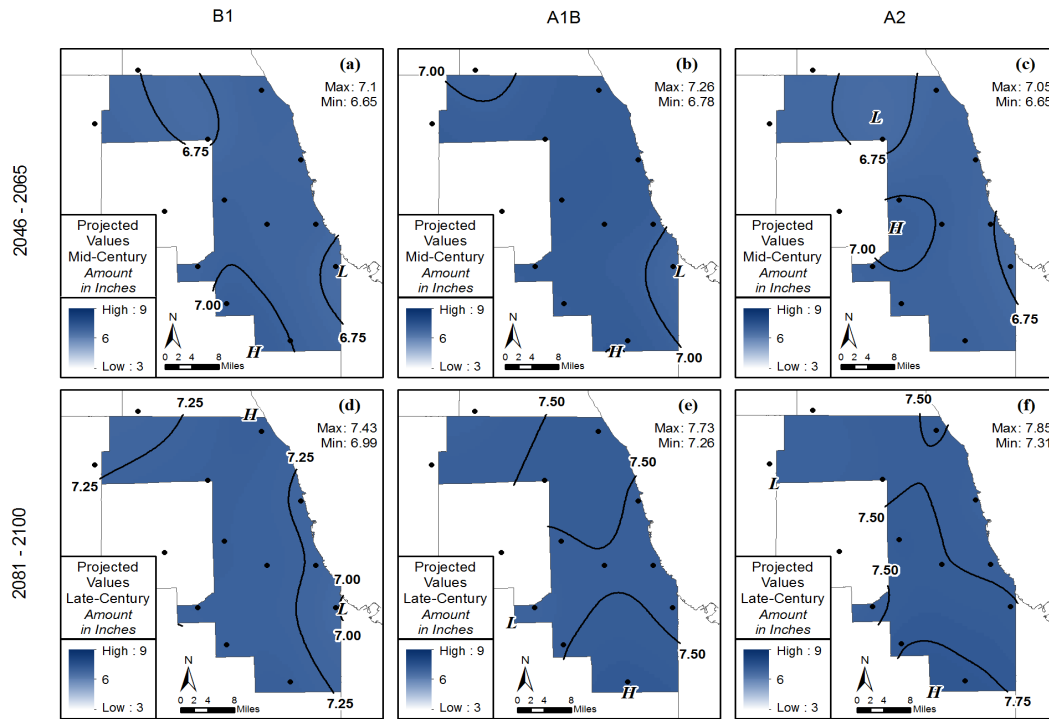


Figure 15 Isohyetals for projected 100-year 24-hour precipitation events

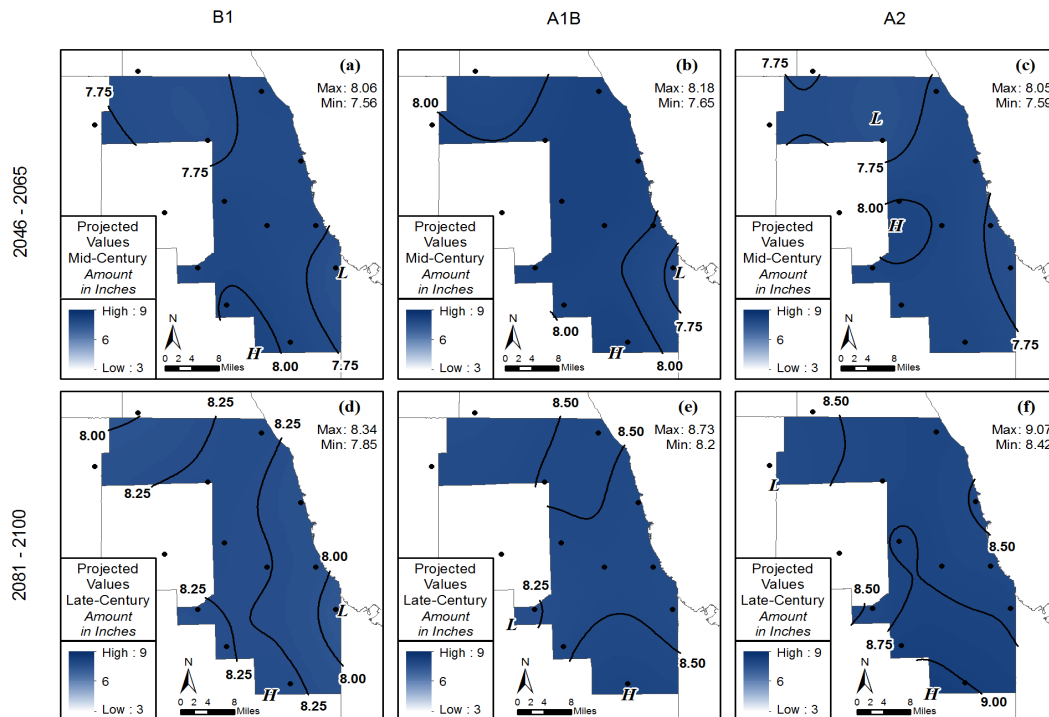


Figure 16 Illustration of Monte Carlo simulation in RFA

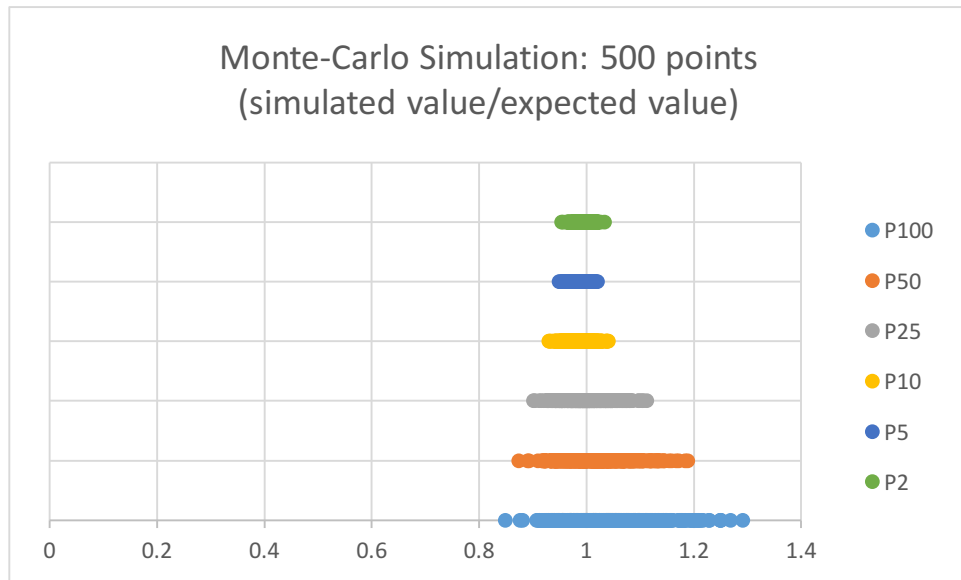


Figure 17 Projected CI for 100-year 24-hour precipitation events (site average, A1B)

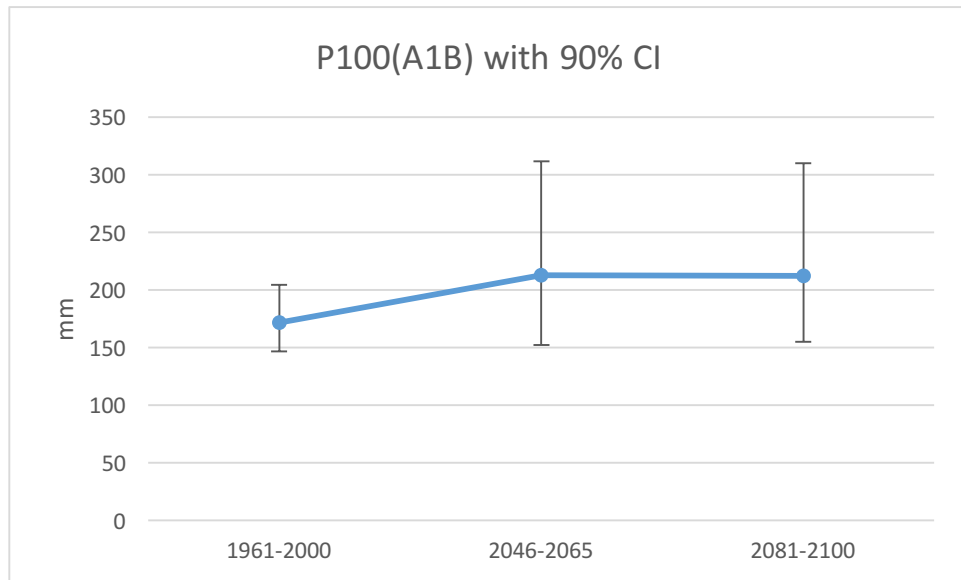


Figure 18 Projected CI for 100-year 24-hour precipitation events (site average, A2)

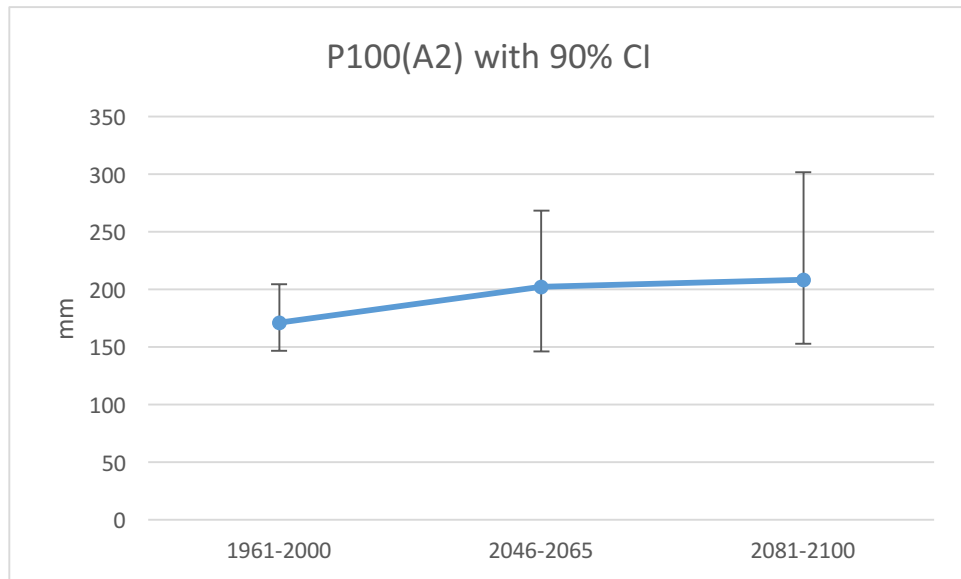


Figure 19 Projected CI for 100-year 24-hour precipitation events (site average, B1)

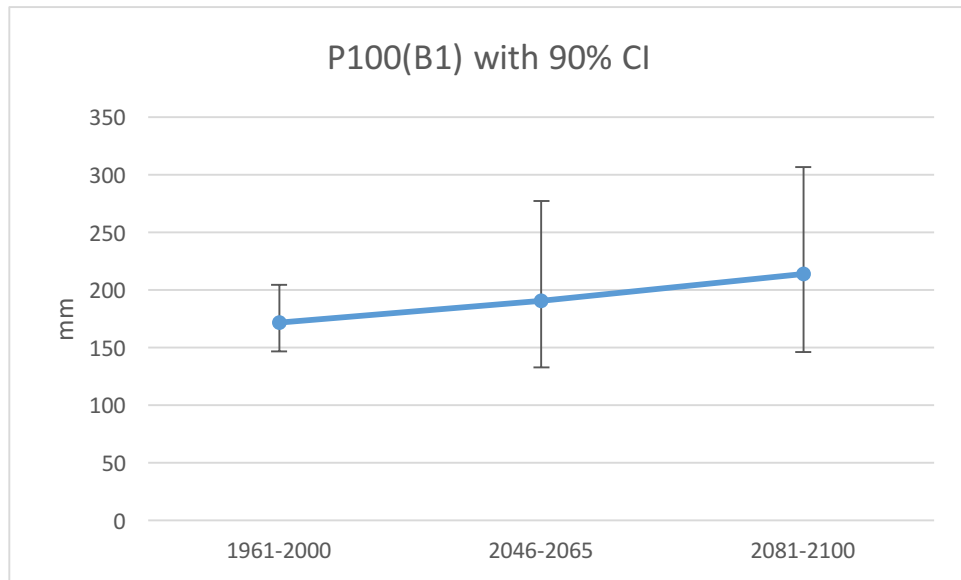


Figure 20 Projected CI for 2-year 24-hour precipitation events (site average, A2)

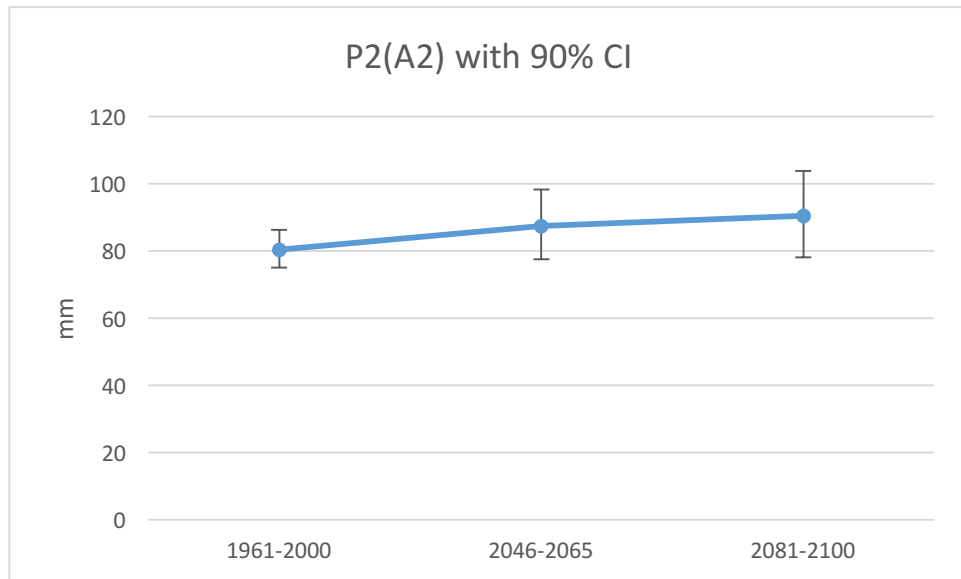


Figure 21 Projected CI for 2-year 24-hour precipitation events (site average, B1)

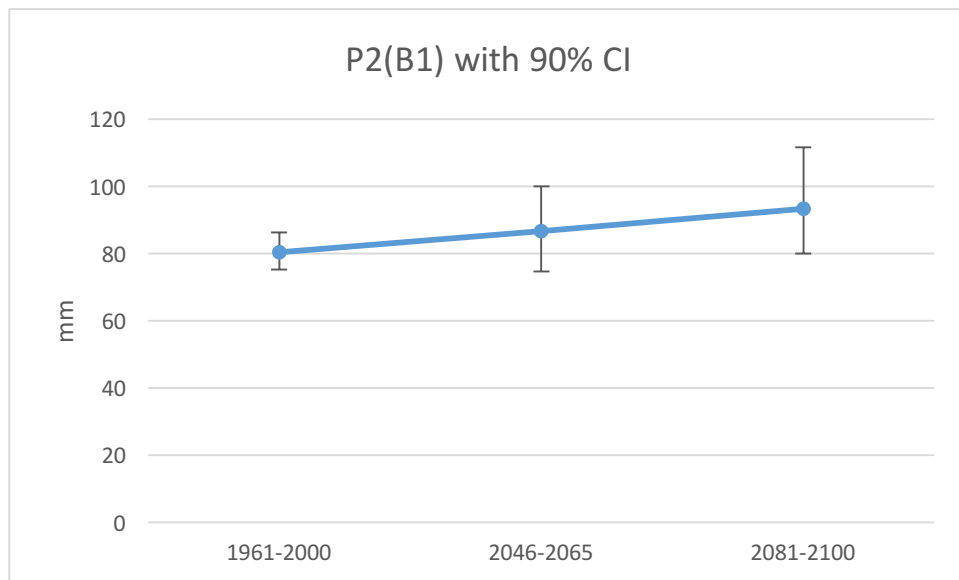


Figure 22 Projected CI for 2-year 24-hour precipitation events (site average, A1B)

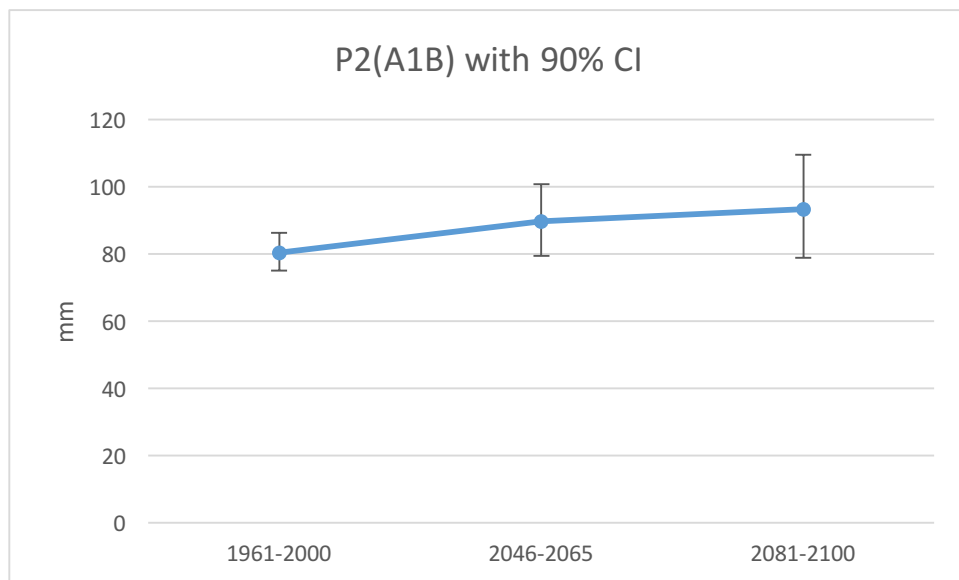


Figure 23 Sample CI vs sample+sampling CI (100-year 24-hour event)

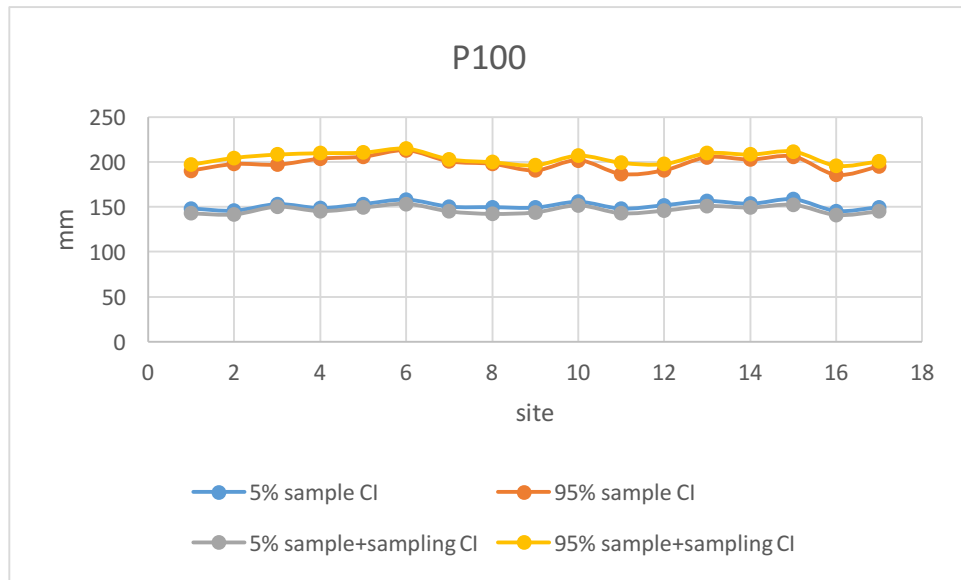


Figure 24 Sample CI vs sample+sampling CI (50-year 24-hour event)

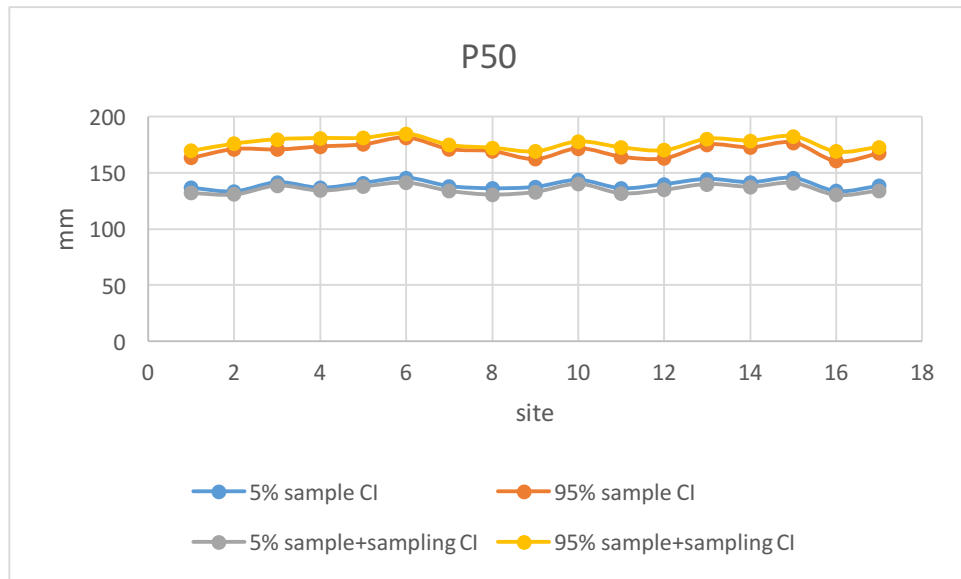


Figure 25 Sample CI vs sample+sampling CI (25-year 24-hour event)

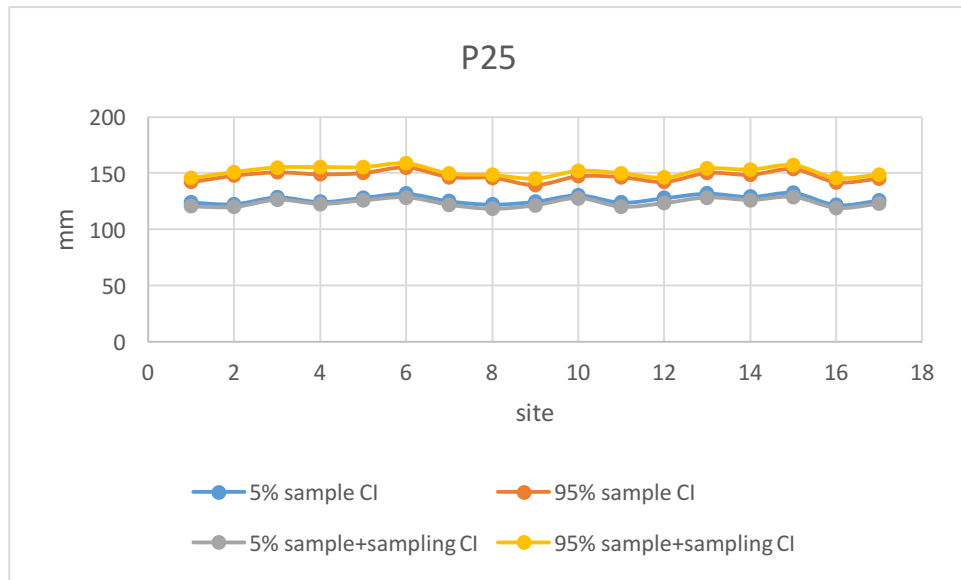


Figure 26 Sample CI vs sample+sampling CI (10-year 24-hour event)

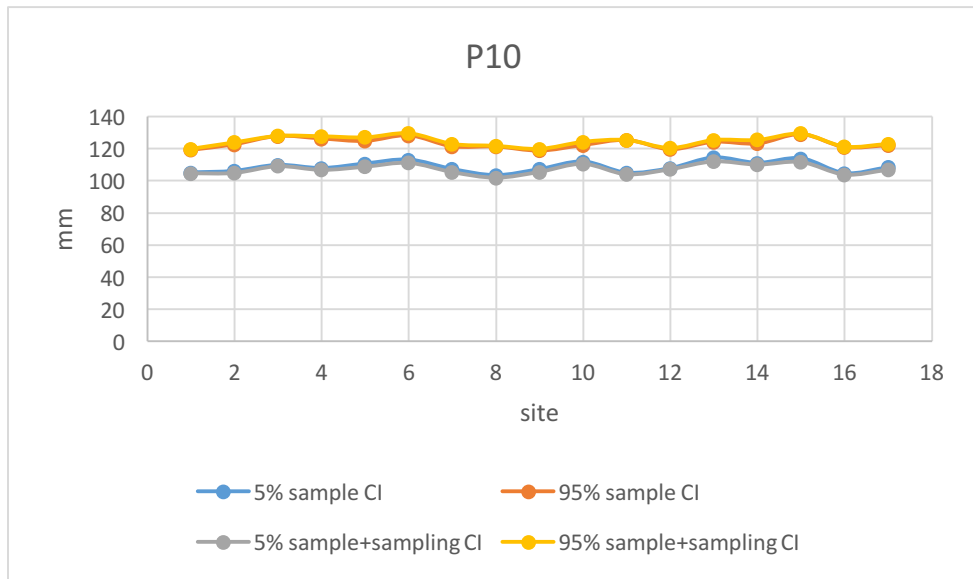




Figure 27 Sample CI vs sample+sampling CI (5-year 24-hour event)

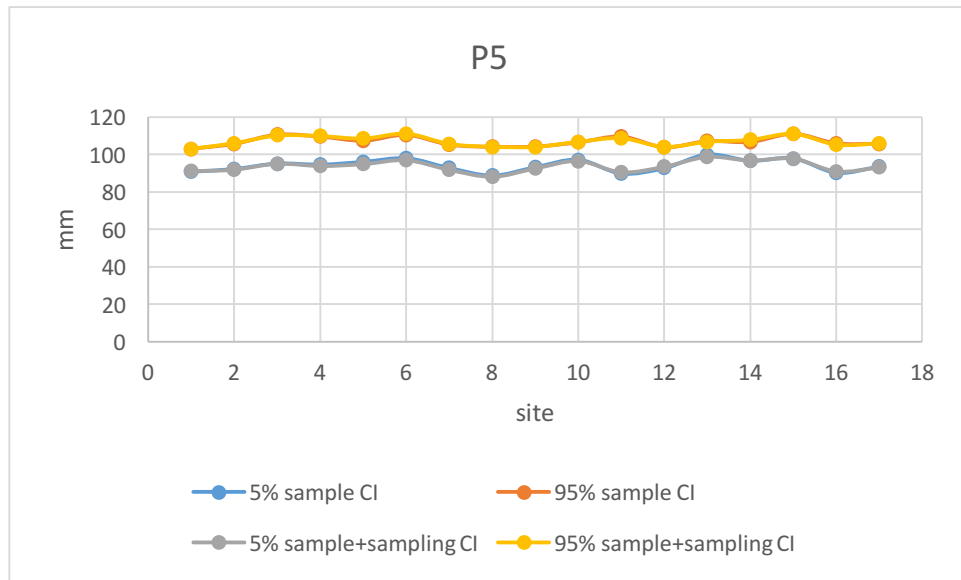


Figure 28 Sample CI vs sample+sampling CI (2-year 24-hour event)

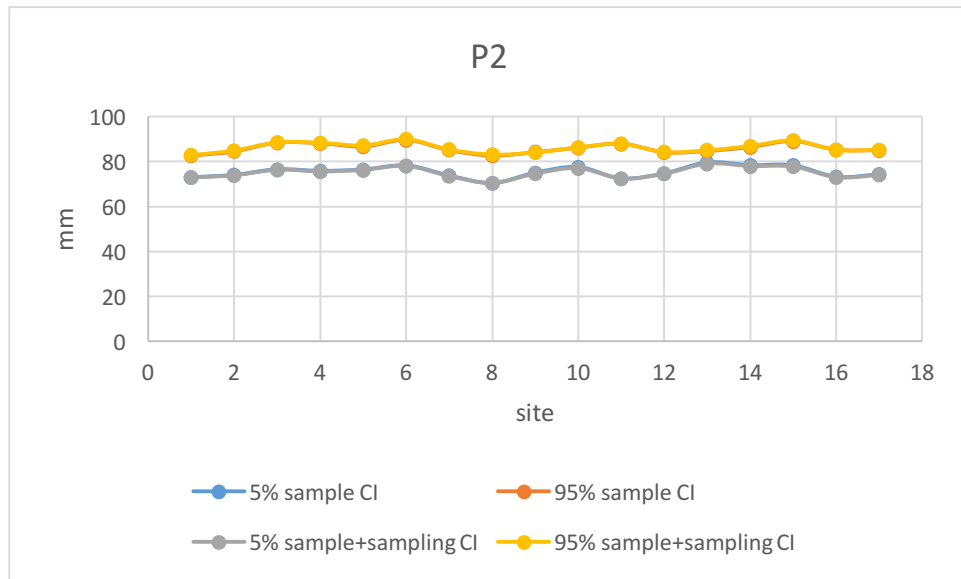


Figure 29 Weighted ensemble vs NOAA Atlas 14 (estimates, 100-year 24-hour event, 2050s)

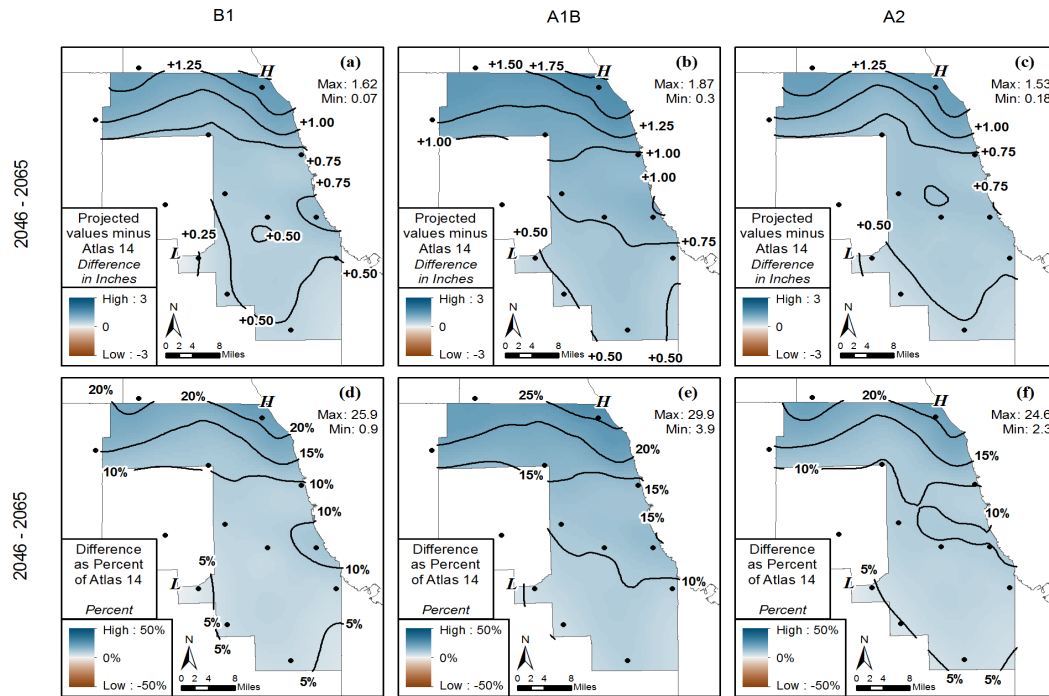


Figure 30 Weighted ensemble vs NOAA Atlas 14 (estimates, 100-year 24-hour event, 2100s)

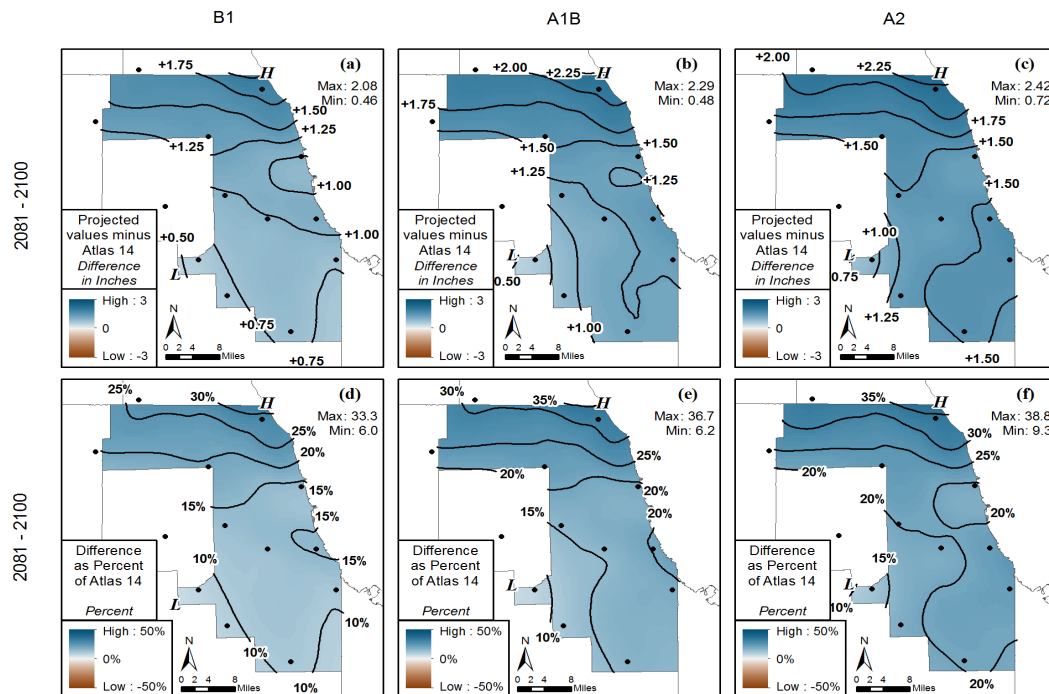


Figure 31 Weighted ensemble vs NOAA Atlas 14 (estimates, 2-year 24-hour event, 2050s)

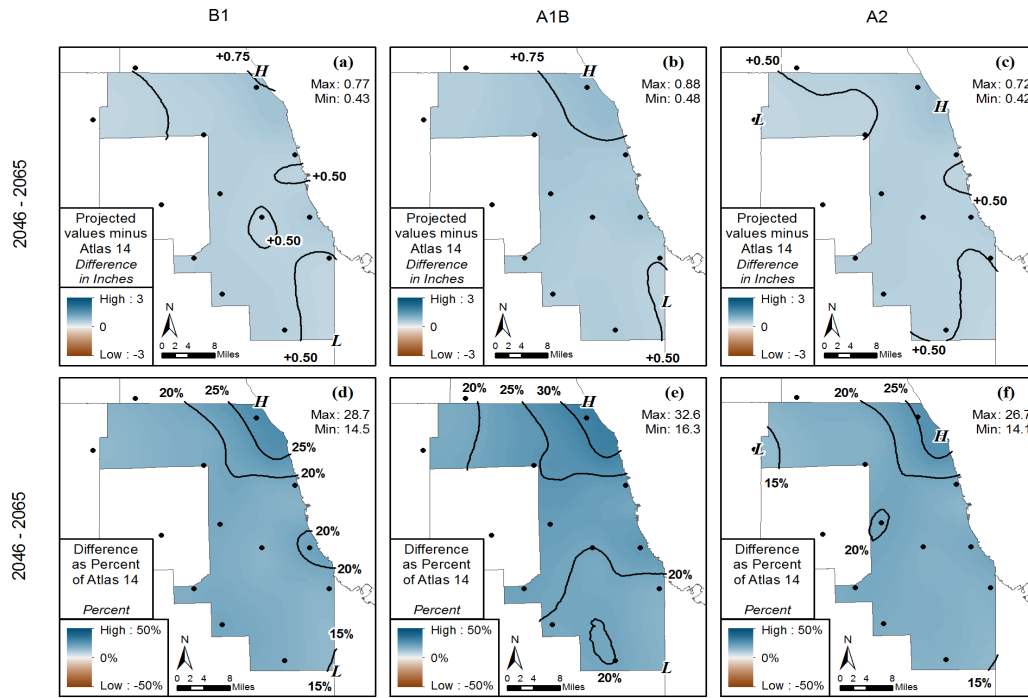


Figure 32 Weighted ensemble vs NOAA Atlas 14 (estimates, 2-year 24-hour event, 2100s)

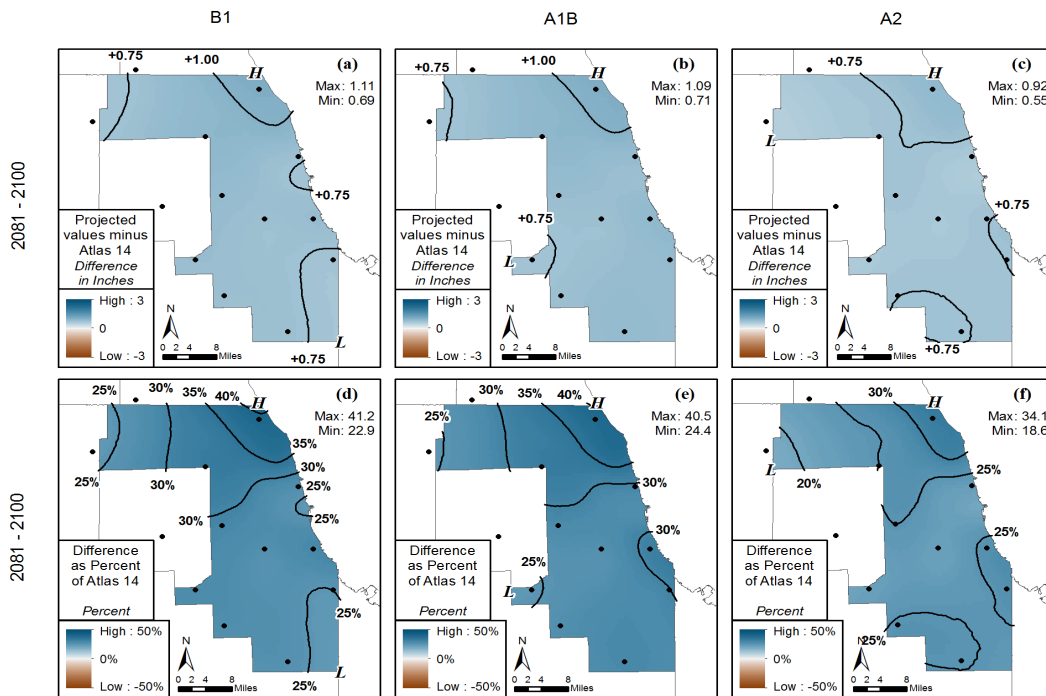


Figure 33 Weighted ensemble vs NOAA Atlas 14 (upper CI, 100-year 24-hour event, 2050s)

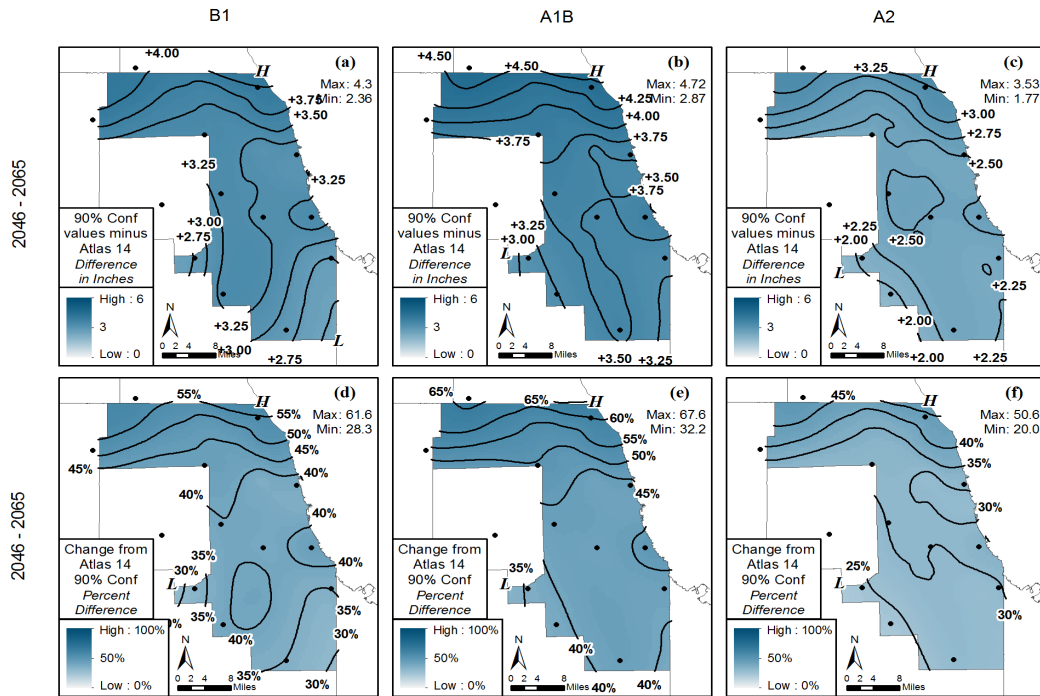


Figure 34 Weighted ensemble vs NOAA Atlas 14 (upper CI, 100-year 24-hour event, 2100s)

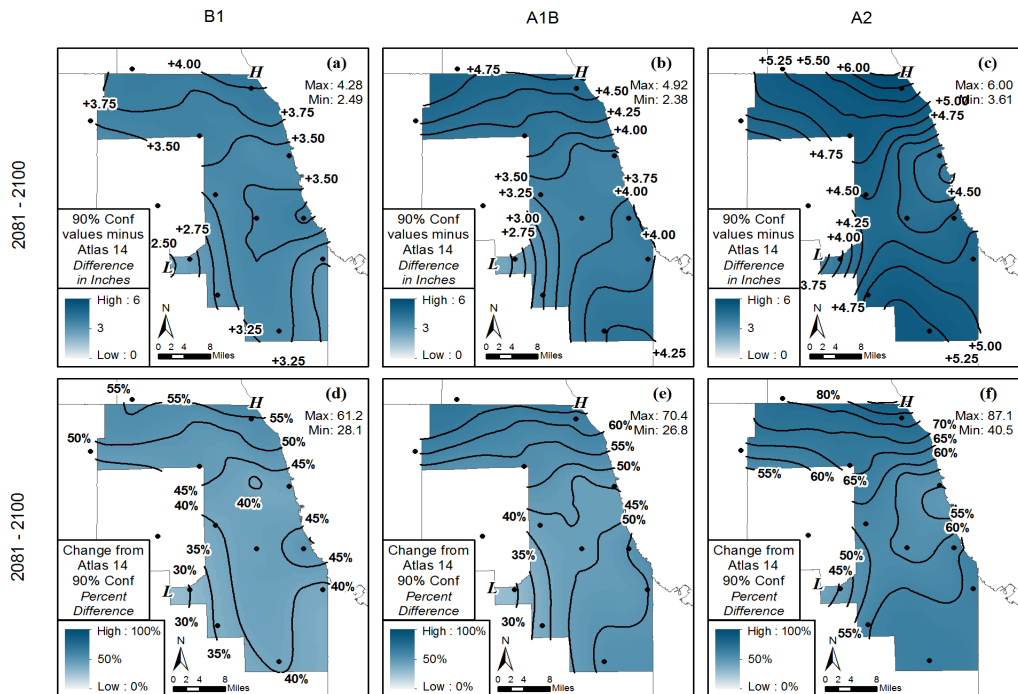


Figure 35 Weighted ensemble vs NOAA Atlas 14 (upper CI, 2-year 24-hour event, 2050s)

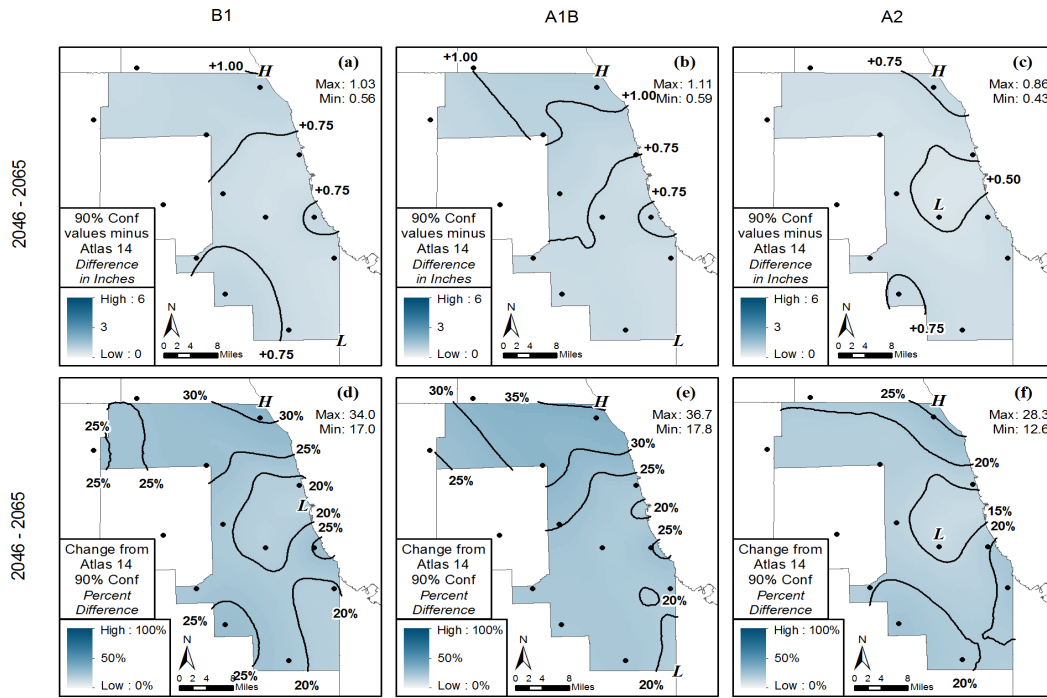


Figure 36 Weighted ensemble vs NOAA Atlas 14 (upper CI, 2-year 24-hour event, 2100s)

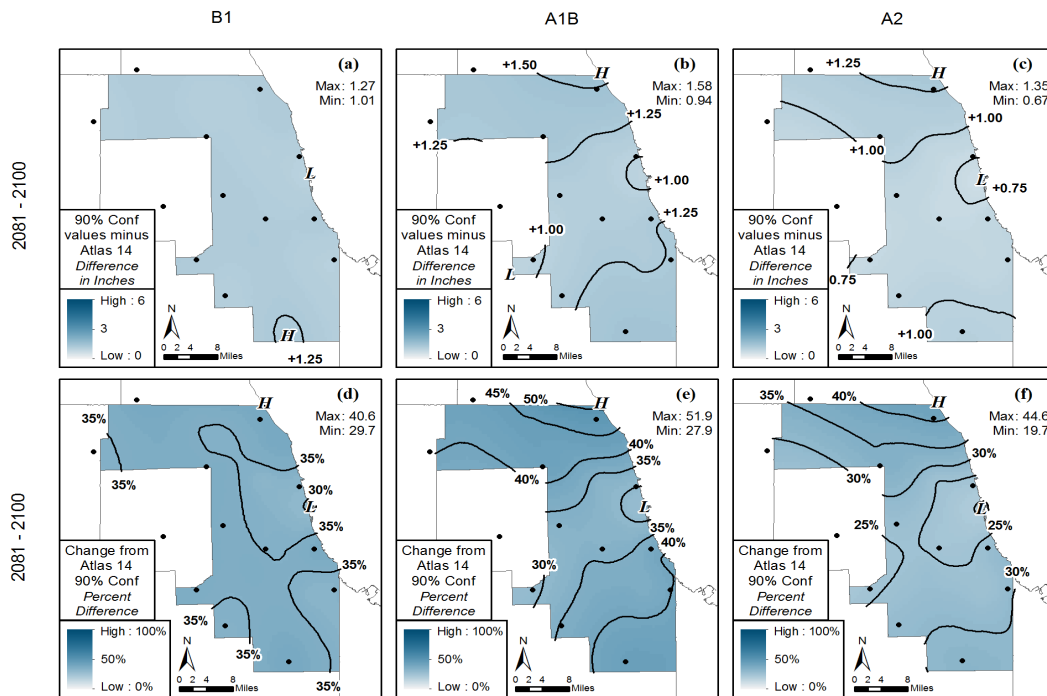


Figure 37 MEM weighting result (V=10)

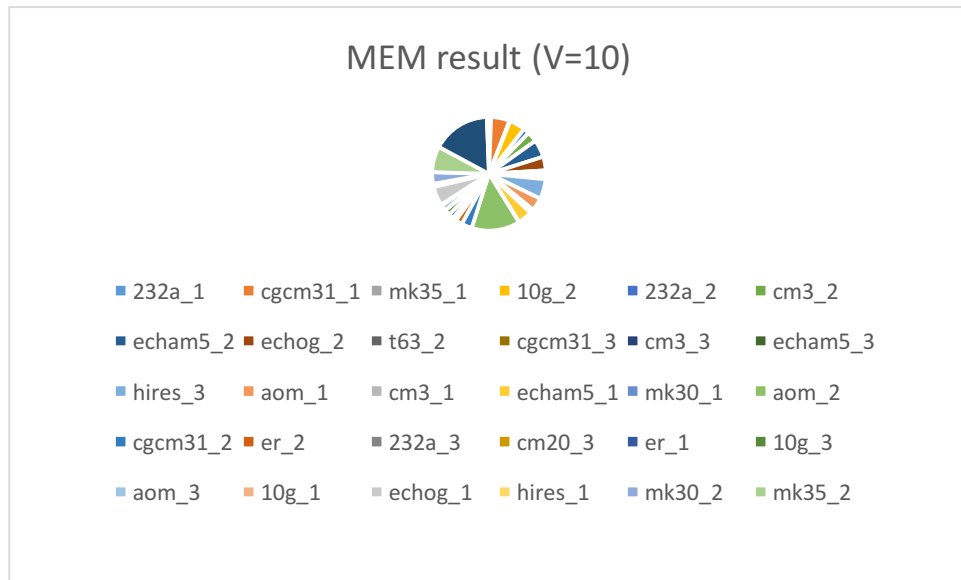


Figure 38 MEM weighting result (V=5)

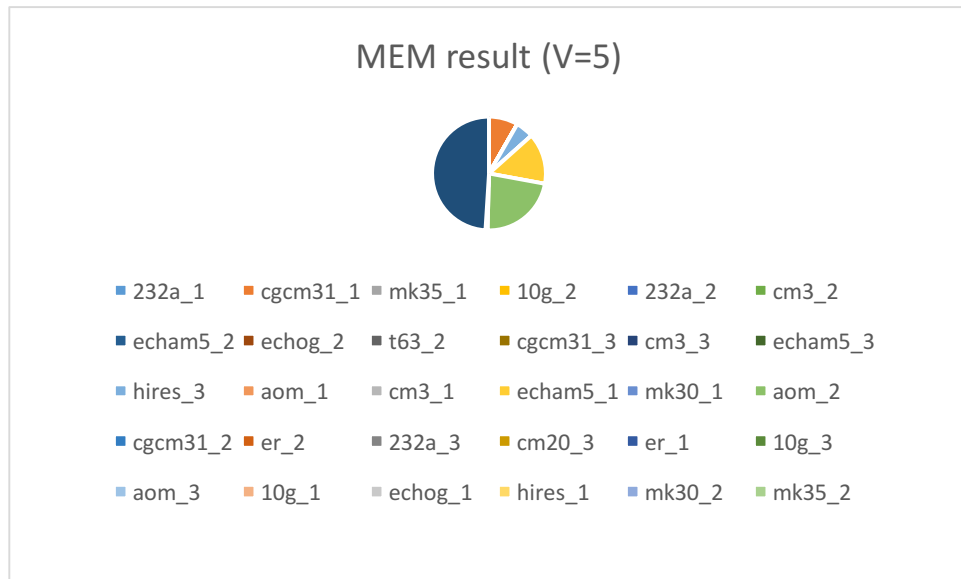


Figure 39 MEM weighting result (V=2)

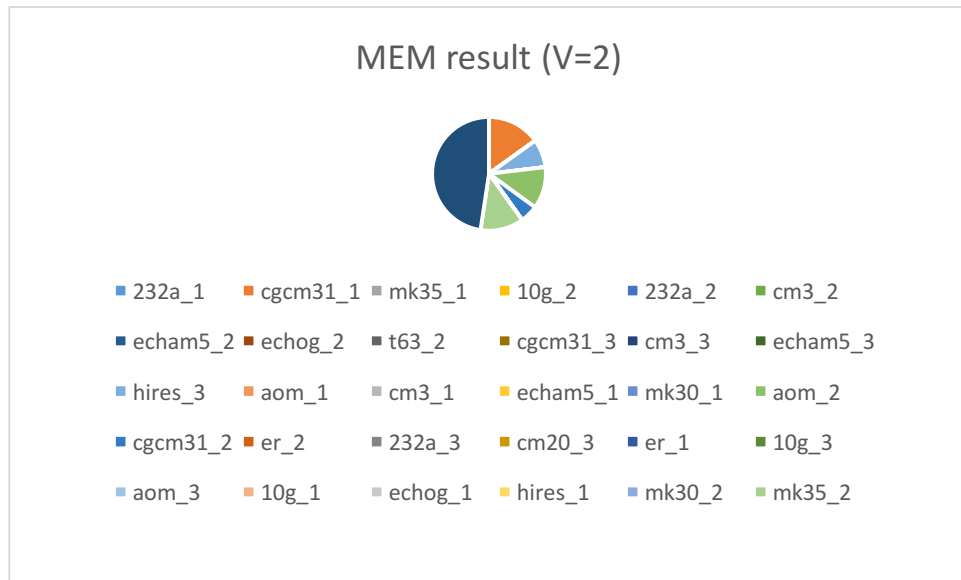
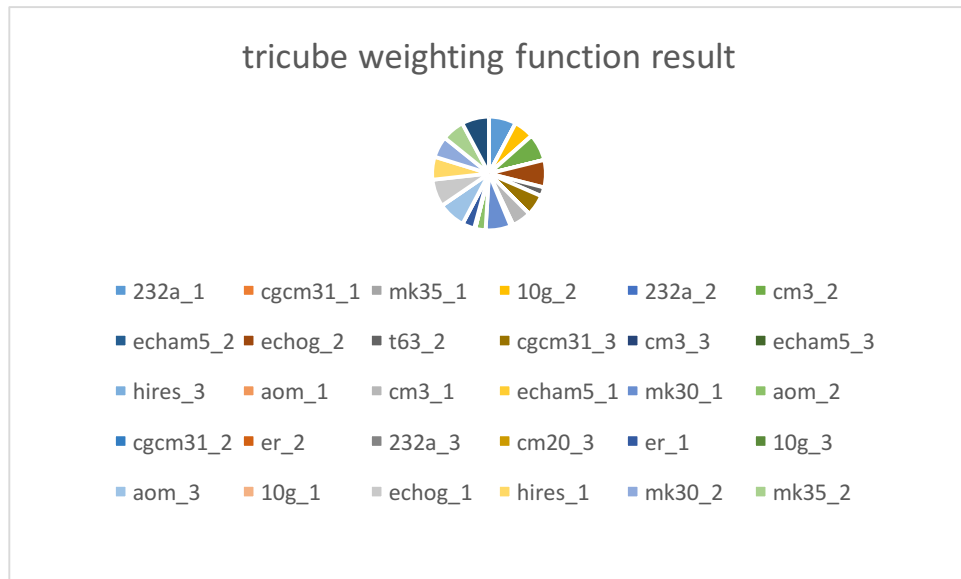


Figure 40 WEM weighting result



## Chapter 7 Tables

Table 1 Comparison between statistical downscaling and dynamical downscaling (Source: Fowler, 2007)

	Statistical downscaling	Dynamical downscaling
<b>Advantages</b>	<ul style="list-style-type: none"> <li>• Comparatively cheap and computationally efficient</li> <li>• Can provide point-scale climatic variables from GCM-scale output</li> <li>• Can be used to derive variables not available from RCMs</li> <li>• Easily transferable to other regions</li> <li>• Based on standard and accepted statistical procedures</li> <li>• Able to directly incorporate observations into method</li> </ul>	<ul style="list-style-type: none"> <li>• Produces responses based on physically consistent processes</li> <li>• Produces finer resolution information from GCM-scale output that can resolve atmospheric processes on a smaller scale</li> </ul>
<b>Disadvantages</b>	<ul style="list-style-type: none"> <li>• Require long and reliable observed historical data series for calibration</li> <li>• Dependent upon choice of predictors</li> <li>• Non-stationarity in the predictor-predictand relationship</li> <li>• Climate system feedbacks not included</li> <li>• Dependent on GCM boundary forcing; affected by biases in underlying GCM</li> <li>• Domain size, climatic region and season affects downscaling skill</li> </ul>	<ul style="list-style-type: none"> <li>• Computationally intensive</li> <li>• Limited number of scenario ensembles available</li> <li>• Strongly dependent on GCM boundary forcing</li> </ul>



Table 2 Description of sites

station name(city)	station ID	longitude	latitude	record length	county	dataset	agency
BARRINGTON	11-0442	-88.1639	42.1153	1963-2012	Cook	NCDC	NOAA
ELGIN	11-2736	-88.2861	42.0628	1899-2012	Kane	NCDC	NOAA
WHEATON 3 SE	11-9221	-88.0728	41.8128	1936-2011	DuPage	NCDC	NOAA
JOLIET	11-4535	-88.1667	41.5000	1894-1974	Will	NCDC	NOAA
JOLIET BRANDON RD DAM	11-4530	-88.1028	41.5033	1943-2012	Will	NCDC	NOAA
PARK FOREST	11-6616	-87.6800	41.4933	1953-2012	Cook	NCDC	NOAA
HOBART 2 WNW	12-4008	-87.2881	41.5422	1920-1999	Lake(Indiana)	NCDC	NOAA
GARY	12-3213	-87.3833	41.6167	1937-1978	Lake(Indiana)	NCDC	NOAA
CHICAGO UNIVERSITY	11-1572	-87.6000	41.7833	1926-1994	Cook	NCDC	NOAA
CHICAGO MIDWAY AP 3 SW	11-1577	-87.7775	41.7372	1928-2012	Cook	NCDC	NOAA
CHICAGO BOTANICAL GARDEN	11-1497	-87.7667	42.1167	1982-2012	Cook	NCDC	NOAA
CHICAGO O'HARE WSO ARP	11-1549	-87.9336	41.9950	1940-2012	Cook	NCDC	NOAA
CHICAGO	7	-87.6451	41.9431	1990-2012	Cook	CCPN	MRCC
WESTBROOK	8	-87.8821	41.8448	1990-2012	Cook	CCPN	MRCC
LEMONT	15	-87.9651	41.6794	1990-2012	Cook	CCPN	MRCC
CHICAGO	19	-87.5397	41.6790	1990-2012	Cook	CCPN	MRCC
ORLAND PARK	20	-87.8758	41.5868	1990-2012	Cook	CCPN	MRCC

Table 3 List of CMIP3 statistical downscaling GCMs

GCM	A1B	A2	B1
cccma_cgcm3_1	O	O	O
cccma_cgcm3_1_t63	O	X	O
cnrm_cm3	O	O	O
csiro_mk3_0	O	O	O
csiro_mk3_5	O	O	O
gfdl_cm2_0	O	O	O
giss_aom	O	X	O
giss_model_e_r	O	O	O
iap_fgoals1_0_g	O	X	O
miroc3_2_hires	O	X	O
miub_echo_g	O	O	O
mpi_echam5	O	O	O
mri_cgcm2_3_2a	O	O	O

Table 4 List of CMIP5 dynamical downscaling GCMs

GCM	RCP8.5
ACCESS	O
BCC-CSM	O
CCSM4	O
CMCC-CM	O
FGOALS	O
GFDL_ESM2M	O
IPSL-CM5A-LR	O
MIROC5	O
MPI-ESM-MR	O
MRI-CGCM3	O
NORES1-M	O

Table 5 WEM estimates of precipitation events (1961-2000, unit: mm)

Site name	p2	p5	p10	p25	p50	p100
Barrington 3 SW IL	77.80	97.03	112.40	133.70	151.93	171.65
Elgin IL	79.87	99.60	115.37	137.23	155.96	176.20
Wheaton 3 SE IL	81.87	102.08	118.23	140.58	159.71	180.38
Joliet IL	81.76	101.96	118.11	140.52	159.73	180.53
Joliet Brandon Rd Dam IL	82.07	102.33	118.53	141.00	160.25	181.08
Park Forest IL	83.62	104.27	120.80	143.74	163.43	184.75
Hobart 2 WNW IN	79.60	99.24	114.96	136.76	155.45	175.67
Gary IN	77.49	96.63	111.94	133.16	151.36	171.05
Site 19 (Chicago, IL)	77.98	97.23	112.60	133.88	152.10	171.80
Chicago Midway Airport 3SW IL	81.72	101.89	118.02	140.39	159.56	180.30
Chicago Botanical Garden IL	79.85	99.56	115.29	137.08	155.73	175.87
Site 7 (Chicago, IL)	79.11	98.64	114.24	135.86	154.38	174.40
Site 8 (Westbrook, IL)	81.37	101.47	117.54	139.81	158.90	179.55
Site 15 (Lemont, IL)	82.22	102.53	118.76	141.27	160.56	181.42
Site 20 (Orland Park, IL)	82.79	103.24	119.58	142.24	161.66	182.66
Chicago O'Hare Int. Airport IL	78.51	97.90	113.38	134.81	153.15	172.97
Chicago University IL	79.13	98.67	114.30	135.98	154.57	174.68

Table 6 Observation estimates of precipitation events (1961-2000, unit: mm)

Site name	p2	p5	p10	p25	p50	p100
Barrington 3 SW IL	77.39	94.92	109.54	131.16	150.96	173.59
Elgin IL	78.47	96.25	111.08	133.00	153.08	176.03
Wheaton 3 SE IL	86.42	106.00	122.33	146.47	168.59	193.86
Joliet IL	77.79	95.41	110.11	131.84	151.75	174.50
Joliet Brandon Rd Dam IL	82.38	101.05	116.61	139.62	160.71	184.80
Park Forest IL	80.53	98.77	113.99	136.48	157.09	180.64
Hobart 2 WNW IN	78.55	96.35	111.19	133.13	153.23	176.21
Gary IN	75.69	92.84	107.14	128.28	147.65	169.79
Site 19 (Chicago, IL)	81.62	100.12	115.54	138.34	159.23	183.10
Chicago Midway Airport 3SW IL	86.52	106.12	122.47	146.64	168.78	194.09
Chicago Botanical Garden IL	79.95	98.06	113.16	135.49	155.95	179.34
Site 7 (Chicago, IL)	77.91	95.56	110.28	132.05	151.99	174.77
Site 8 (Westbrook, IL)	78.61	96.42	111.27	133.23	153.35	176.34
Site 15 (Lemont, IL)	85.05	104.31	120.38	144.14	165.90	190.77
Site 20 (Orland Park, IL)	82.75	101.50	117.13	140.25	161.43	185.63
Chicago O'Hare Int. Airport IL	77.03	94.48	109.03	130.55	150.26	172.79
Chicago University IL	72.50	88.92	102.62	122.87	141.43	162.63

Table 7 WEM estimates of precipitation events (2046-2065, A1B, unit: mm)

Site name	p2	p5	p10	p25	p50	p100
Barrington 3 SW IL	87.24	110.67	129.27	154.59	175.83	198.34
Elgin IL	90.17	114.31	133.44	159.45	181.24	204.33
Wheaton 3 SE IL	90.43	114.74	134.04	160.31	182.34	205.71
Joliet IL	87.85	111.45	130.15	155.57	176.87	199.42
Joliet Brandon Rd Dam IL	87.50	111.03	129.68	155.06	176.32	198.85
Park Forest IL	91.29	115.77	135.16	161.53	183.61	207.01
Hobart 2 WNW IN	87.31	110.67	129.18	154.34	175.42	197.75
Gary IN	85.59	108.48	126.60	151.19	171.77	193.55
Site 19 (Chicago, IL)	85.81	108.88	127.17	152.09	173.01	195.20
Chicago Midway Airport 3SW IL	90.50	114.82	134.08	160.24	182.14	205.32
Chicago Botanical Garden IL	90.76	115.12	134.41	160.65	182.64	205.95
Site 7 (Chicago, IL)	90.40	114.68	133.91	160.02	181.88	205.02
Site 8 (Westbrook, IL)	90.95	115.42	134.81	161.18	183.26	206.63
Site 15 (Lemont, IL)	90.24	114.52	133.77	159.97	181.94	205.22
Site 20 (Orland Park, IL)	89.78	113.94	133.08	159.08	180.85	203.90
Chicago O'Hare Int. Airport IL	90.29	114.51	133.69	159.79	181.66	204.84
Chicago University IL	89.36	113.38	132.42	158.31	180.01	202.99

Table 8 WEM estimates of precipitation events (2046-2065, A2, unit: mm)

Site name	p2	p5	p10	p25	p50	p100
Barrington 3 SW IL	86.54	108.41	126.03	150.90	172.79	197.14
Elgin IL	86.18	107.92	125.43	150.13	171.83	195.96
Wheaton 3 SE IL	88.77	111.18	129.26	154.80	177.28	202.33
Joliet IL	84.87	106.25	123.50	147.88	169.37	193.30
Joliet Brandon Rd Dam IL	84.69	106.04	123.24	147.53	168.90	192.70
Park Forest IL	89.03	111.50	129.55	154.94	177.22	201.97
Hobart 2 WNW IN	85.55	107.17	124.55	149.07	170.61	194.59
Gary IN	84.32	105.64	122.78	146.94	168.18	191.81
Site 19 (Chicago, IL)	85.69	107.33	124.69	149.11	170.53	194.30
Chicago Midway Airport 3SW IL	88.70	111.12	129.21	154.76	177.25	202.30
Chicago Botanical Garden IL	86.72	108.61	126.27	151.24	173.25	197.78
Site 7 (Chicago, IL)	87.22	109.25	127.02	152.10	174.17	198.75
Site 8 (Westbrook, IL)	89.16	111.71	129.89	155.57	178.18	203.36
Site 15 (Lemont, IL)	88.79	111.21	129.29	154.83	177.31	202.34
Site 20 (Orland Park, IL)	88.77	111.12	129.09	154.41	176.63	201.31
Chicago O'Hare Int. Airport IL	84.97	106.43	123.73	148.15	169.64	193.55
Chicago University IL	86.02	107.73	125.24	149.97	171.75	195.99

Table 9 WEM estimates of precipitation events (2046-2065, B1, unit: mm)

Site name	p2	p5	p10	p25	p50	p100
Barrington 3 SW IL	86.03	108.14	125.76	150.25	171.51	195.00
Elgin IL	87.27	109.76	127.65	152.50	174.05	197.84
Wheaton 3 SE IL	88.24	111.00	129.08	154.15	175.85	199.75
Joliet IL	86.59	108.92	126.69	151.36	172.76	196.39
Joliet Brandon Rd Dam IL	85.76	107.86	125.45	149.89	171.09	194.49
Park Forest IL	89.57	112.52	130.75	155.99	177.82	201.84
Hobart 2 WNW IN	84.99	106.72	123.98	147.92	168.65	191.47
Gary IN	85.35	107.21	124.55	148.56	169.32	192.16
Site 19 (Chicago, IL)	85.22	107.08	124.45	148.56	169.44	192.44
Chicago Midway Airport 3SW IL	87.79	110.39	128.40	153.43	175.17	199.19
Chicago Botanical Garden IL	87.95	110.56	128.57	153.61	175.34	199.34
Site 7 (Chicago, IL)	87.09	109.47	127.28	152.04	173.53	197.27
Site 8 (Westbrook, IL)	88.32	111.06	129.20	154.46	176.42	200.70
Site 15 (Lemont, IL)	88.05	110.72	128.78	153.91	175.73	199.85
Site 20 (Orland Park, IL)	89.92	113.10	131.55	157.20	179.45	204.01
Chicago O'Hare Int. Airport IL	85.77	107.86	125.44	149.85	171.00	194.32
Chicago University IL	87.71	110.23	128.16	153.08	174.71	198.60

Table 10 WEM estimates of precipitation events (2081-2100, A1B, unit: mm)

Site name	p2	p5	p10	p25	p50	p100
Barrington 3 SW IL	93.39	117.89	137.36	164.05	186.64	210.87
Elgin IL	94.19	118.89	138.52	165.42	188.19	212.60
Wheaton 3 SE IL	94.83	119.68	139.44	166.55	189.53	214.18
Joliet IL	91.38	115.33	134.37	160.45	182.53	206.20
Joliet Brandon Rd Dam IL	92.22	116.30	135.44	161.65	183.84	207.62
Park Forest IL	98.00	123.68	144.10	172.08	195.78	221.21
Hobart 2 WNW IN	96.69	122.06	142.26	169.99	193.49	218.71
Gary IN	94.28	119.00	138.69	165.71	188.65	213.29
Site 19 (Chicago, IL)	94.65	119.44	139.14	166.12	188.94	213.38
Chicago Midway Airport 3SW IL	95.29	120.28	140.13	167.30	190.28	214.91
Chicago Botanical Garden IL	96.08	121.23	141.21	168.59	191.75	216.56
Site 7 (Chicago, IL)	95.23	120.18	140.01	167.18	190.18	214.84
Site 8 (Westbrook, IL)	95.15	120.12	139.96	167.13	190.13	214.78
Site 15 (Lemont, IL)	92.73	117.02	136.30	162.66	184.92	208.74
Site 20 (Orland Park, IL)	95.19	120.14	139.95	167.05	189.96	214.48
Chicago O'Hare Int. Airport IL	95.86	120.97	140.93	168.25	191.36	216.13
Chicago University IL	95.05	119.93	139.70	166.80	189.75	214.34



Table 11 WEM estimates of precipitation events (2081-2100, A2, unit: mm)

Site name	p2	p5	p10	p25	p50	p100
Barrington 3 SW IL	90.39	114.48	134.10	162.07	187.05	215.43
Elgin IL	89.76	113.74	133.23	160.96	185.67	213.67
Wheaton 3 SE IL	90.41	114.66	134.46	162.78	188.20	217.20
Joliet IL	88.44	112.21	131.53	159.04	183.58	211.44
Joliet Brandon Rd Dam IL	90.66	115.02	134.86	163.15	188.45	217.22
Park Forest IL	95.25	120.85	141.73	171.56	198.28	228.69
Hobart 2 WNW IN	93.68	118.81	139.29	168.52	194.67	224.41
Gary IN	90.68	115.01	134.80	163.01	188.19	216.78
Site 19 (Chicago, IL)	92.02	116.75	136.89	165.64	191.35	220.56
Chicago Midway Airport 3SW IL	91.98	116.63	136.72	165.43	191.12	220.35
Chicago Botanical Garden IL	91.72	116.31	136.38	165.07	190.77	220.02
Site 7 (Chicago, IL)	90.18	114.30	133.95	161.95	186.95	215.33
Site 8 (Westbrook, IL)	92.73	117.63	137.96	167.06	193.17	222.96
Site 15 (Lemont, IL)	90.51	114.84	134.64	162.86	188.08	216.74
Site 20 (Orland Park, IL)	94.11	119.43	140.11	169.72	196.29	226.62
Chicago O'Hare Int. Airport IL	90.53	114.78	134.60	163.02	188.53	217.65
Chicago University IL	91.26	115.73	135.63	163.97	189.27	218.01

Table 12 WEM estimates of precipitation events (2081-2100, B1, unit: mm)

Site name	p2	p5	p10	p25	p50	p100
Barrington 3 SW IL	92.66	116.51	135.05	160.02	180.86	202.92
Elgin IL	93.78	117.96	136.74	162.03	183.11	205.40
Wheaton 3 SE IL	97.11	122.21	141.73	168.05	190.02	213.32
Joliet IL	91.86	115.57	134.03	158.99	179.90	202.12
Joliet Brandon Rd Dam IL	90.95	114.43	132.70	157.38	178.04	199.97
Park Forest IL	96.03	120.84	140.13	166.16	187.90	210.93
Hobart 2 WNW IN	91.84	115.51	133.94	158.86	179.72	201.88
Gary IN	90.74	114.13	132.34	156.91	177.44	199.21
Site 19 (Chicago, IL)	91.12	114.59	132.85	157.50	178.11	199.97
Chicago Midway Airport 3SW IL	95.42	120.09	139.30	165.20	186.85	209.80
Chicago Botanical Garden IL	96.44	121.29	140.59	166.59	188.29	211.26
Site 7 (Chicago, IL)	93.33	117.45	136.25	161.67	182.95	205.56
Site 8 (Westbrook, IL)	95.82	120.56	139.81	165.77	187.45	210.44
Site 15 (Lemont, IL)	95.29	119.85	138.93	164.61	186.02	208.67
Site 20 (Orland Park, IL)	95.32	119.92	139.04	164.83	186.36	209.18
Chicago O'Hare Int. Airport IL	95.98	120.74	139.99	165.95	187.63	210.60
Chicago University IL	93.37	117.53	136.35	161.77	183.04	205.61

Table 13 WEM estimates of 90% CI (2046-2065, A1B, unit: mm)

Site No.	P100_L	P100_U	P50_L	P50_U	P25_L	P25_U	P10_L	P10_U	P5_L	P5_U	P2_L	P2_U
1	138.70	295.37	129.17	246.05	118.79	205.03	104.33	162.93	91.74	136.21	73.35	105.56
2	147.15	290.94	137.21	241.10	126.30	199.40	111.07	157.46	98.04	131.47	79.05	102.63
3	134.53	300.96	124.73	249.28	114.69	206.23	101.06	162.92	89.63	136.05	74.29	105.07
4	143.76	288.19	134.41	238.67	124.18	197.25	109.32	154.11	97.17	127.53	78.99	98.34
5	139.71	290.09	130.48	240.15	119.47	197.46	105.80	155.12	94.14	128.44	76.88	99.18
6	152.02	298.24	141.54	246.19	130.50	203.10	114.83	159.12	101.77	132.06	83.35	102.43
7	142.63	278.33	132.95	229.45	122.20	188.39	107.68	147.23	96.22	121.12	77.92	96.66
8	144.29	272.62	135.10	225.70	124.52	186.32	110.03	146.38	96.95	121.48	77.79	94.90
9	132.44	283.84	123.45	234.36	113.80	193.66	100.92	152.12	90.14	126.53	74.19	98.66
10	143.38	297.86	133.66	246.48	122.82	203.80	108.48	160.92	96.33	134.20	78.48	104.32
11	142.77	297.94	132.84	246.71	122.11	204.27	109.24	159.79	96.41	133.58	77.27	105.55
12	142.62	296.75	132.92	245.76	122.30	203.11	107.90	160.49	95.71	134.11	77.21	104.14
13	143.13	303.20	133.08	251.11	122.45	208.22	107.95	164.11	95.75	136.79	78.00	106.10
14	140.48	299.72	130.86	247.33	120.34	204.02	106.35	159.56	94.64	132.18	77.74	102.49
15	144.86	298.68	135.10	247.09	124.57	204.37	109.74	159.98	97.79	132.71	79.77	102.33
16	141.31	297.08	131.09	246.56	120.09	204.75	105.16	162.74	94.28	135.22	75.43	107.32
17	139.94	291.78	130.78	242.05	120.77	200.32	106.91	157.47	95.13	130.80	77.54	101.38

Table 14 WEM estimates of 90% CI (2046-2065, A2, unit: mm)

Site No.	P100_L	P100_U	P50_L	P50_U	P25_L	P25_U	P10_L	P10_U	P5_L	P5_U	P2_L	P2_U
1	142.44	264.18	133.33	217.96	123.15	180.22	108.42	142.62	95.36	120.42	76.54	96.49
2	146.71	263.34	137.50	218.37	126.44	181.13	110.68	144.62	97.58	122.60	76.94	98.10
3	141.56	269.40	132.51	222.96	122.44	184.43	108.02	146.08	95.35	124.26	76.78	100.26
4	144.97	258.20	135.79	212.96	125.50	175.57	110.24	138.15	96.89	116.73	77.01	93.91
5	145.59	256.85	136.78	212.09	126.15	174.74	110.76	137.41	97.07	115.76	76.63	92.74
6	153.38	268.90	143.09	222.90	131.83	185.47	115.52	148.67	100.58	126.43	79.48	100.86
7	141.76	262.41	131.82	217.64	123.13	180.38	107.93	145.22	95.09	124.50	76.42	99.86
8	141.59	258.45	132.00	214.16	123.35	177.57	108.42	142.34	95.53	121.43	76.49	96.81
9	145.06	257.94	135.16	214.06	124.40	178.52	109.30	144.15	95.92	123.78	75.96	99.45
10	145.07	273.23	135.66	225.32	125.00	185.86	109.85	146.51	96.72	123.16	78.78	97.77
11	142.83	267.80	133.32	221.33	121.90	182.46	107.01	144.62	94.23	122.47	75.99	98.65
12	145.68	270.26	135.50	223.34	124.35	184.76	108.76	146.38	95.45	123.50	76.90	98.50
13	142.97	275.28	133.27	226.71	122.64	186.95	107.16	146.78	94.69	121.86	77.14	98.26
14	144.89	273.44	135.33	226.27	124.55	187.68	109.31	149.21	96.03	126.58	77.71	100.45
15	150.16	265.54	139.85	220.11	128.36	183.72	114.06	149.11	100.30	129.70	78.93	104.49
16	137.35	260.55	128.23	215.32	118.09	178.52	103.85	142.50	91.35	121.16	74.21	96.29
17	143.27	263.70	133.96	218.11	123.53	180.60	108.46	143.46	95.18	121.42	76.18	97.00

Table 15 WEM estimates of 90% CI (2046-2065, B1, unit: mm)

Site No.	P100_L	P100_U	P50_L	P50_U	P25_L	P25_U	P10_L	P10_U	P5_L	P5_U	P2_L	P2_U
1	135.61	281.06	125.22	230.80	114.86	190.83	101.50	151.78	90.25	128.07	73.63	100.19
2	136.13	288.03	125.71	237.06	115.34	196.48	101.97	156.41	90.31	131.90	73.70	103.04
3	139.69	293.41	129.68	242.69	119.51	202.00	105.65	161.57	93.48	135.95	75.46	105.37
4	137.68	289.48	128.00	237.92	117.85	196.91	104.43	157.65	92.94	133.34	75.53	103.77
5	137.11	285.00	127.41	233.79	117.17	192.92	103.54	153.66	91.86	129.25	74.74	100.51
6	145.75	280.85	135.66	231.66	124.53	191.64	108.94	153.29	95.07	129.64	76.04	102.25
7	139.93	263.94	130.24	217.20	119.53	179.15	104.65	143.15	91.43	121.35	73.29	96.68
8	139.63	265.30	130.06	218.44	119.23	180.96	104.23	144.68	90.99	122.53	72.79	96.96
9	133.68	269.05	124.07	220.91	113.87	182.60	100.07	145.82	87.81	123.20	70.95	97.08
10	138.08	291.36	130.53	239.45	119.70	197.04	105.00	155.87	92.58	130.50	75.31	101.45
11	137.69	287.47	128.08	237.18	117.60	195.73	103.13	155.54	91.41	131.20	74.66	103.09
12	139.12	284.68	129.54	234.30	118.60	193.24	104.05	153.07	91.76	128.44	74.50	100.65
13	136.62	295.38	126.25	242.67	118.49	198.91	103.96	157.06	91.82	131.47	74.92	102.45
14	136.92	291.39	126.60	239.56	116.25	198.26	102.60	157.37	90.93	132.07	74.34	102.78
15	139.52	300.87	129.04	248.09	118.35	205.73	104.06	164.09	91.84	137.79	74.53	107.21
16	132.97	284.57	123.18	235.04	112.92	195.00	98.73	155.55	87.27	131.17	71.16	102.64
17	137.36	283.90	127.50	233.74	116.87	193.57	102.49	154.05	90.11	129.65	73.09	101.87

Table 16 WEM estimates of 90% CI (2081-2100, A1B, unit: mm)

Site No.	P100_L	P100_U	P50_L	P50_U	P25_L	P25_U	P10_L	P10_U	P5_L	P5_U	P2_L	P2_U
1	145.99	300.46	134.26	251.61	121.93	211.79	108.28	169.04	95.52	143.86	78.09	114.03
2	149.26	305.21	137.61	256.19	125.02	215.40	108.65	173.77	95.31	146.98	77.00	115.29
3	151.06	299.30	139.59	249.80	127.62	209.53	112.08	168.67	99.37	142.78	81.07	112.09
4	149.73	290.77	138.54	244.04	126.63	205.08	110.54	165.01	97.03	139.01	77.80	108.05
5	154.77	284.97	143.10	238.46	130.62	200.05	113.90	161.34	99.99	136.83	80.13	107.69
6	154.90	315.97	142.80	265.46	129.93	223.57	113.24	180.84	99.47	153.17	80.37	120.22
7	152.45	315.41	140.93	264.60	128.76	222.19	112.31	178.44	98.53	150.10	79.54	116.75
8	149.60	308.22	138.45	258.82	126.43	217.60	110.54	175.44	97.11	147.73	78.06	114.71
9	151.85	298.57	140.29	251.15	128.00	211.37	111.57	170.58	97.90	144.52	78.98	113.78
10	153.03	302.39	141.28	253.58	128.60	213.35	112.41	172.49	99.40	146.29	81.33	115.32
11	151.77	302.95	140.38	254.50	128.64	215.06	112.40	174.64	99.12	148.46	80.31	116.82
12	155.18	300.30	143.31	250.35	130.38	209.18	115.55	165.56	101.90	140.03	83.06	110.53
13	151.95	302.71	140.20	253.07	127.61	212.34	113.35	168.82	99.90	142.72	80.25	112.76
14	153.03	285.49	141.58	239.70	130.19	202.02	113.70	163.26	99.93	138.37	80.40	108.48
15	152.07	298.47	141.59	252.64	128.75	212.38	112.11	172.20	98.21	145.80	79.24	114.16
16	153.35	304.80	141.86	255.40	129.33	214.65	113.04	173.45	99.63	146.78	80.99	115.82
17	154.03	297.93	142.28	248.92	129.95	208.36	113.87	167.67	100.74	142.10	81.81	112.15

Table 17 WEM estimates of 90% CI (2081-2100, A2, unit: mm)

Site No.	P100_L	P100_U	P50_L	P50_U	P25_L	P25_U	P10_L	P10_U	P5_L	P5_U	P2_L	P2_U
1	151.53	310.86	140.32	252.85	128.20	206.83	111.63	163.32	97.24	138.20	77.23	109.46
2	154.74	307.14	143.74	249.42	130.84	203.23	115.23	160.31	100.51	135.02	79.10	105.58
3	154.04	322.87	143.00	259.58	131.59	209.32	114.93	159.90	101.17	131.15	80.73	102.04
4	148.38	308.63	136.27	247.96	126.45	199.03	110.08	152.73	95.98	127.96	78.18	99.73
5	150.38	320.37	137.69	257.47	127.63	206.77	110.83	159.03	96.45	133.68	78.70	104.44
6	157.27	342.39	144.27	275.30	131.19	222.41	114.46	171.81	100.92	142.00	81.56	110.67
7	153.49	329.63	141.89	265.95	128.72	214.97	111.77	166.14	97.94	137.51	78.82	107.49
8	148.74	316.06	136.41	254.58	124.23	206.64	108.69	160.91	95.84	134.61	77.66	105.92
9	145.59	322.50	133.96	259.29	121.80	209.25	107.39	157.87	94.29	131.19	76.12	104.66
10	153.55	322.70	143.28	260.35	133.33	210.16	117.09	162.54	103.59	135.76	82.33	106.82
11	150.75	331.66	138.36	267.96	128.14	217.74	109.58	170.15	96.21	141.91	76.65	110.99
12	150.05	310.34	139.29	250.20	127.21	202.34	111.91	157.66	98.69	132.06	78.65	104.34
13	155.60	332.80	145.60	268.79	134.87	217.01	118.28	166.58	104.41	137.43	84.04	107.21
14	149.73	321.48	137.26	258.60	127.26	208.08	110.51	160.21	97.14	133.19	78.49	104.16
15	153.99	344.73	143.28	277.03	129.90	221.64	112.03	168.30	96.49	139.63	78.35	108.13
16	149.67	329.83	137.28	265.93	124.63	215.67	107.98	167.45	94.50	139.14	75.49	109.11
17	151.89	314.03	141.08	253.27	128.93	204.31	114.14	155.89	100.21	129.79	79.59	103.16

Table 18 WEM estimates of 90% CI (2081-2100, B1, unit: mm)

Site No.	P100_L	P100_U	P50_L	P50_U	P25_L	P25_U	P10_L	P10_U	P5_L	P5_U	P2_L	P2_U
1	141.96	276.29	132.99	235.61	123.31	201.05	109.43	164.39	97.76	139.89	80.53	110.86
2	140.88	278.81	131.68	237.42	121.54	201.81	109.62	162.34	97.51	138.56	80.16	109.89
3	145.04	299.56	135.89	255.46	126.80	217.76	112.27	176.58	99.78	149.09	81.86	116.69
4	139.15	289.18	131.51	249.69	121.40	213.16	107.10	173.69	94.77	146.88	77.33	115.04
5	136.49	284.25	128.91	244.49	118.76	207.95	104.53	168.74	92.47	142.42	75.35	111.56
6	139.91	293.37	131.33	250.27	121.94	213.18	108.74	173.69	97.18	147.57	80.20	116.19
7	141.97	284.91	133.22	241.59	123.24	204.28	109.52	164.75	97.91	139.02	80.54	109.30
8	136.03	273.18	127.80	232.16	118.74	196.82	106.00	159.36	94.86	134.93	77.92	106.29
9	139.92	276.20	131.27	235.28	121.57	199.94	107.48	162.09	95.09	137.11	77.56	108.15
10	142.53	299.42	133.59	255.35	123.61	217.12	109.25	175.99	97.26	148.68	79.23	116.28
11	147.21	287.69	137.26	244.08	126.36	206.36	113.24	164.17	100.21	138.75	81.36	109.08
12	140.05	292.57	131.52	248.93	122.06	211.06	108.62	170.36	96.75	143.34	79.17	111.93
13	145.07	295.77	135.98	252.13	125.82	214.35	111.18	173.74	98.44	146.64	80.55	115.04
14	146.46	287.16	137.14	244.98	126.73	208.60	111.92	169.94	99.35	144.55	81.79	114.84
15	143.96	293.93	134.34	249.76	123.68	212.54	110.97	170.51	97.95	144.00	79.48	112.68
16	145.13	291.60	135.51	247.86	127.83	207.40	112.58	167.48	100.06	141.57	81.75	111.01
17	141.86	294.44	133.46	250.85	124.05	212.92	110.47	171.87	98.39	144.28	80.60	111.82



Table 19 Comparison between WEM and MEM performance (100-year 24-hour event, unit: mm)

Site name	Observation	WEM	V=10	v=5	V=2
Barrington 3 SW IL	173.59	171.65	174.87	177.84	172.91
Elgin IL	176.03	176.20	178.11	178.56	173.66
Wheaton 3 SE IL	193.86	180.38	186.05	188.06	185.09
Joliet IL	174.50	180.53	181.50	179.74	176.85
Joliet Brandon Rd Dam IL	184.80	181.08	182.24	179.62	176.57
Park Forest IL	180.64	184.75	186.96	186.47	182.99
Hobart 2 WNW IN	176.21	175.67	178.84	181.64	176.93
Gary IN	169.79	171.05	173.56	172.42	171.09
Site 19 (Chicago, IL)	183.10	171.80	176.76	180.64	174.20
Chicago Midway Airport 3SW IL	194.09	180.30	184.40	184.42	177.18
Chicago Botanical Garden IL	179.34	175.87	179.99	184.64	180.30
Site 7 (Chicago, IL)	174.77	174.40	177.74	177.92	171.89
Site 8 (Westbrook, IL)	176.34	179.55	184.43	184.47	178.70
Site 15 (Lemont, IL)	190.77	181.42	186.16	186.48	182.84
Site 20 (Orland Park, IL)	185.63	182.66	185.16	182.35	180.45
Chicago O'Hare Int. Airport IL	172.79	172.97	175.98	177.00	173.25
Chicago University IL	162.63	174.68	174.52	170.80	164.98

## References

IPCC, edited.

Allan, R. P., and B. J. Soden (2008), Atmospheric warming and the amplification of precipitation extremes, *Science*, 321(5895), 1481-1484.

Annamalai, H., K. Hamilton, and K. R. Sperber (2007), The South Asian summer monsoon and its relationship with ENSO in the IPCC AR4 simulations, *Journal of Climate*, 20(6), 1071-1092.

Ashfaq, M., L. C. Bowling, K. Cherkauer, J. S. Pal, and N. S. Diffenbaugh (2010), Influence of climate model biases and daily - scale temperature and precipitation events on hydrological impacts assessment: A case study of the United States, *Journal of Geophysical Research: Atmospheres* (1984–2012), 115(D14).

Ashfaq, M., S. Ghosh, S. C. Kao, L. C. Bowling, P. Mote, D. Touma, S. A. Rauscher, and N. S. Diffenbaugh (2013), Near - term acceleration of hydroclimatic change in the western US, *Journal of Geophysical Research: Atmospheres*, 118(19).

Bhaskaran, B., and J. F. B. Mitchell (1998), Simulated changes in Southeast Asian monsoon precipitation resulting from anthropogenic emissions, *International Journal of Climatology*, 18(13), 1455-1462.

Bonnin, G. M., D. Martin, B. Lin, T. Parzybok, M. Yekta, and D. Riley (2006), Precipitation-frequency atlas of the United States, *NOAA atlas*, 14(2).

Change, C. (2007), Intergovernmental Panel on Climate Change, *World Meteorological*

### *Organization.*

De Fraiture, C. (2003), The use of entropy optimization principles in parameter estimation: applications to global water and food modeling, Ph. D. Dissertation submitted to the Faculty of the Graduate School of the University of Colorado, Department of Civil Environmental Architectural Engineering, Colorado, p 165.

Flato, G., J. Marotzke, B. Abiodun, P. Braconnot, S. C. Chou, W. Collins, P. Cox, F. Driouech, S. Emori, and V. Eyring (2013), Evaluation of climate models, in *Climate change 2013: the physical science basis. Contribution of Working Group I to the Fifth Assessment Report of the Intergovernmental Panel on Climate Change*, edited, pp. 741-866, Cambridge University Press.

Fowler, H. J., S. Blenkinsop, and C. Tebaldi (2007), Linking climate change modelling to impacts studies: recent advances in downscaling techniques for hydrological modelling, *International journal of climatology*, 27(12), 1547-1578.

Gain, A. K., W. W. Immerzeel, F. C. Spera Weiland, and M. F. P. Bierkens (2011), Impact of climate change on the stream flow of the lower Brahmaputra: trends in high and low flows based on discharge-weighted ensemble modelling, *Hydrology and Earth System Sciences*, 15(5), 1537-1545.

Giorgi, F., L. O. Mearns, C. Shields, and L. McDaniel (1998), Regional nested model simulations of present day and 2× CO<sub>2</sub> climate over the central plains of the US, *Climatic Change*, 40(3-4), 457-493.

Gleckler, P. J., K. E. Taylor, and C. Doutriaux (2008), Performance metrics for climate models,

*Journal of Geophysical Research: Atmospheres*, 113(D6).

Greenwood, J. A., J. M. Landwehr, N. C. Matalas, and J. R. Wallis (1979), Probability weighted moments: definition and relation to parameters of several distributions expressible in inverse form, *Water Resources Research*, 15(5), 1049-1054.

Grotch, S. L., and M. C. MacCracken (1991), The use of general circulation models to predict regional climatic change, *Journal of Climate*, 4(3), 286-303.

Hanssen-Bauer, I., C. Achberger, R. E. Benestad, D. Chen, and E. J. Forland (2005), Statistical downscaling of climate scenarios over Scandinavia, *Climate Research*, 29(3), 255.

Hennegriff, W. (2007), Climate change and floods--findings and adaptation strategies for flood protection in Baden-Württemberg, *Water Science & Technology*, 56(4).

Hennessy, K. J., J. M. Gregory, and J. F. B. Mitchell (1997), Changes in daily precipitation under enhanced greenhouse conditions, *Climate Dynamics*, 13(9), 667-680.

Hewitson, B. C., and R. G. Crane (1996), Climate downscaling: techniques and application, *Climate Research*, 7(2), 85-95.

Hosking, J. R. M. (2015), Regional frequency analysis using L-moments. R package, version 3.0-1, edited.

Hosking, J. R. M., and J. R. Wallis (1993), Some statistics useful in regional frequency analysis, *Water Resources Research*, 29(2), 271-281.

Hosking, J. R. M., and J. R. Wallis (2005), *Regional frequency analysis: an approach based on L-moments*, Cambridge University Press.

Huff, F. A., and J. R. Angel (1989), *Frequency distributions and hydroclimatic characteristics of heavy rainstorms in Illinois*, Illinois State Water Survey.

ISWS, edited.

Jaynes, E. T. (1978), Where do we stand on maximum entropy, *The maximum entropy formalism*, 15-118.

Jun, M., R. Knutti, and D. W. Nychka (2008), Spatial analysis to quantify numerical model bias and dependence: how many climate models are there?, *Journal of the American Statistical Association*, 103(483), 934-947.

Kim, J. (2005), A projection of the effects of the climate change induced by increased CO<sub>2</sub> on extreme hydrologic events in the western US, *Climatic Change*, 68(1-2), 153-168.

Kothavala, Z. (1997), Extreme precipitation events and the applicability of global climate models to the study of floods and droughts, *Mathematics and computers in simulation*, 43(3), 261-268.

Kotir, J. H. (2011), Climate change and variability in Sub-Saharan Africa: a review of current and future trends and impacts on agriculture and food security, *Environment, Development and Sustainability*, 13(3), 587-605.

Kunkel, K. E., R. Moss, and A. Parris (2015), Innovations in science and scenarios for assessment, *Climatic Change*, 1-14.

Langbein, W. B. (1949), Annual floods and the partial - duration flood series, *Eos, Transactions American Geophysical Union*, 30(6), 879-881.

Laurent, R., and X. Cai (2007), A maximum entropy method for combining AOGCMs for regional

intra-year climate change assessment, *Climatic change*, 82(3-4), 411-435.

Lynch, S. D. (1998), Converting point estimates of daily rainfall onto a rectangular grid, *Department of Agricultural Engineering, University of Natal, South Africa*.

Markus, M., J. R. Angel, L. Yang, and M. I. Hejazi (2007), Changing estimates of design precipitation in Northeastern Illinois: Comparison between different sources and sensitivity analysis, *Journal of hydrology*, 347(1), 211-222.

Meehl, G. A., F. Zwiers, J. Evans, T. Knutson, L. Mearns, and P. Whetton (2000), Trends in extreme weather and climate events: Issues related to modeling extremes in projections of future climate change\*, *Bulletin of the American Meteorological Society*, 81(3), 427-436.

Meehl, G. A., C. Covey, K. E. Taylor, T. Delworth, R. J. Stouffer, M. Latif, B. McAvaney, and J. F. B. Mitchell (2007), The WCRP CMIP3 multimodel dataset: A new era in climate change research, *Bulletin of the American Meteorological Society*, 88(9), 1383-1394.

Mosteller, F., and J. W. Tukey (1977), Data analysis and regression: a second course in statistics, *Addison-Wesley Series in Behavioral Science: Quantitative Methods*.

Murphy, J. M., D. M. H. Sexton, D. N. Barnett, G. S. Jones, M. J. Webb, M. Collins, and D. A. Stainforth (2004), Quantification of modelling uncertainties in a large ensemble of climate change simulations, *Nature*, 430(7001), 768-772.

Nakicenovic, N., and R. Swart (2000), Special report on emissions scenarios, *Special Report on Emissions Scenarios, Edited by Nebojsa Nakicenovic and Robert Swart, pp. 612. ISBN 0521804930. Cambridge, UK: Cambridge University Press, July 2000., 1.*

Nguyen, V. T. V. (2005), Downscaling methods for evaluating the impacts of climate change and variability on hydrological regime at basin scale, paper presented at International Symposium on Role of Water Sciences in Transboundary River Basin Management, Thailand.

NOAA, edited.

Nohara, D., A. Kitoh, M. Hosaka, and T. Oki (2006), Impact of climate change on river discharge projected by multimodel ensemble, *Journal of Hydrometeorology*, 7(5), 1076-1089.

Notaro, M., D. Lorenz, C. Hoving, and M. Schummer (2014), Twenty-First-Century Projections of Snowfall and Winter Severity across Central-Eastern North America\*,+, *Journal of Climate*, 27(17), 6526-6550.

Olesen, J. E., and M. Bindi (2002), Consequences of climate change for European agricultural productivity, land use and policy, *European journal of agronomy*, 16(4), 239-262.

Oubeidillah, A. A., S. C. Kao, M. Ashfaq, B. S. Naz, and G. Tootle (2014), A large-scale, high-resolution hydrological model parameter data set for climate change impact assessment for the conterminous US, *Hydrology and Earth System Sciences*, 18(1), 67-84.

Pennell, C., and T. Reichler (2011), On the effective number of climate models, *Journal of Climate*, 24(9), 2358-2367.

Perica, S., D. Martin, S. Pavlovic, I. Roy, M. St Laurent, C. Trypaluk, D. Unruh, M. Yekta, and G. Bonnin (2013), NOAA Atlas 14 Volume 9 Version 2. Precipitation-frequency atlas of the United States, southeastern states, *NOAA, National Weather Service, Silver Spring, MD*.

Rajczak, J., P. Pall, and C. Schär (2013), Projections of extreme precipitation events in regional

climate simulations for Europe and the Alpine Region, *Journal of Geophysical Research: Atmospheres*, 118(9), 3610-3626.

Ray, A. J., J. J. Barsugli, K. B. Averyt, K. Wolter, M. Hoerling, N. Doesken, B. Udall, and R. S. Webb (2008), Climate change in Colorado: a synthesis to support water resources management and adaptation, *Report for the Colorado Water Conservation Board. University of Colorado, Boulder*.

Rimoldini, L. (2013), Weighted skewness and kurtosis unbiased by sample size, *arXiv preprint arXiv:1304.6564*.

Rosenthal, E. (2008), GAMS-A user's guide, paper presented at GAMS Development Corporation, Citeseer.

Salathé, E. P. (2003), Comparison of various precipitation downscaling methods for the simulation of streamflow in a rainshadow river basin, *International Journal of Climatology*, 23(8), 887-901.

Sanderson, B. M., R. Knutti, and P. Caldwell (2015), A representative democracy to reduce interdependency in a multimodel ensemble, *Journal of Climate*, 28(13), 5171-5194.

Schuster, Z. T., K. W. Potter, and D. S. Liebl (2011), Assessing the effects of climate change on precipitation and flood damage in Wisconsin, *Journal of Hydrologic Engineering*, 17(8), 888-894.

Shannon, C. E. (2001), A mathematical theory of communication, *ACM SIGMOBILE Mobile Computing and Communications Review*, 5(1), 3-55.

Tramblay, Y., W. Badi, F. Driouech, S. El Adlouni, L. Neppel, and E. Servat (2012), Climate change impacts on extreme precipitation in Morocco, *Global and Planetary Change*, 82, 104-114.



Wehner, M. F. (2013), Very extreme seasonal precipitation in the NARCCAP ensemble: model performance and projections, *Climate Dynamics*, 40(1-2), 59-80.

Wilby, R. L., and T. M. L. Wigley (1997), Downscaling general circulation model output: a review of methods and limitations, *Progress in Physical Geography*, 21(4), 530-548.

Wilby, R. L., D. Conway, and P. D. Jones (2002), Prospects for downscaling seasonal precipitation variability using conditioned weather generator parameters, *Hydrological Processes*, 16(6), 1215-1234.

Wilby, R. L., S. P. Charles, E. Zorita, B. Timbal, P. Whetton, and L. O. Mearns (2004), Guidelines for use of climate scenarios developed from statistical downscaling methods.

Winters, B. A., J. R. Angel, C. Ballerine, J. Byard, A. Flegel, D. Gambill, E. Jenkins, S. A. McConkey, M. Markus, and B. A. Bender (2015), Report for the Urban Flooding Awareness ActRep., Illinois Department of Natural Resources.

Xu, C.-y. (1999), From GCMs to river flow: a review of downscaling methods and hydrologic modelling approaches, *Progress in Physical Geography*, 23(2), 229-249.

Zhang, X. (2010), Impacts of climate change on global agricultural land availability, University of Illinois at Urbana-Champaign.

Zorita, E., and H. Von Storch (1999), The analog method as a simple statistical downscaling technique: comparison with more complicated methods, *Journal of climate*, 12(8), 2474-2489.